Till-forming processes beneath parts of the Cordilleran Ice Sheet, British Columbia, Canada: macroscale and microscale evidence and a new statistical technique for analysing microstructure data

CHRISTINA M. NEUDORF, TRACY A. BRENNAND AND OLAV B. LIAN

This paper presents the first integrated macroscale and microscale examination of subglacial till associated with the last-glacial (Fraser Glaciation) Cordilleran Ice Sheet (CIS). A new statistical approach to quantifying till micromorphology (multivariate hierarchical cluster analysis for compositional data) is also described and implemented. Till macrostructures, macrofabrics and microstructures support previous assertions that primary till in this region formed through a combination of lodgement and deformation processes in a temperate subglacial environment. Macroscale observations suggest that subglacial environments below the CIS were probably influenced by topography, whereby poor drainage of the substrate in topographically constricted areas, or on slopes adverse to the ice-flow direction at glacial maximum, facilitated ductile deformation of the glacier bed. Microscale observations suggest that subglacial till below the CIS experienced both ductile and brittle deformation, including grain rotation and squeeze flow of sediment between grains under moist conditions, and microshearing, grain stacking and grain fracturing under well-drained conditions. Macroscale observations suggest that ductile deformation events were probably followed by brittle deformation events as the substrate subsequently drained. The prevalence of ductile-type microstructures in most till exposures investigated in this study suggests that ductile deformation signatures can be preserved at the microscale after brittle deformation events that result in larger-scale fractures and shear structures. It is likely that microscale ductile deformation can also occur within distributed shear zones during lodgement processes. Cluster analysis of microstructure data and qualitative observations made from thin sections suggest that the relative frequency of countable microstructures in this till is influenced by topography in relation to ice-flow direction (bed drainage conditions) as well as by the frequency and distribution of voids in the till matrix and skeletal grain shapes.

Christina M. Neudorf (christina.neudorf@ufv.ca) and Olav B. Lian, Department of Geography, University of the Fraser Valley, Abbotsford, British Columbia, Canada, V2S 7M8; Tracy A. Brennand, Department of Geography, Simon Fraser University, Burnaby, British Columbia, Canada, V5A 1S6; received 9th March 2012, accepted 21st December 2012.

Understanding the ice-flow dynamics of ancient ice sheets requires an understanding of the processes that operated at the glacier bed. Sedimentological and geological data from the beds of ancient glaciers and ice sheets are crucial for developing models that predict changes in the stability of modern-day ice sheets and how they will impact global climate and sea level (Alley & Bindschadler 2001; Bertler & Barrett 2010). In the 1980s the importance of subglacial sediments, especially till, in governing ice-flow dynamics was realised, motivating detailed sedimentological studies into tills associated with ancient continental ice sheets in order to aid reconstructions of past ice-flow dynamics (e.g. Boulton & Jones 1979; Boulton & Hindmarsh 1987; Hart & Boulton 1991; Hicock & Dreimanis 1992; Hart 1994; Hicock & Fuller 1995). Glaciotectonic studies of deposits associated with the Cordilleran Ice Sheet (CIS) have been conducted along the west coast of British Columbia (BC) (Hicock & Dreimanis 1985; Brown *et al.* 1987; Parkin & Hicock 1989; Hicock & Fuller 1995; Hicock & Lian 1999; Lian & Hicock 2010) and in the interior of BC (Broster *et al.* 1979; Broster & Clague 1987; Broster 1991; Huntley & Broster 1993; Lian &

Hicock 2000; Lian *et al.* 2003). This work has focused largely on the sedimentology, architecture, macro-(pebble-) fabric and structural geology of glacigenic sediments and glacially affected bedrock as observed in the field at the macroscale. Glacial micromorphology is becoming an increasingly popular tool for unravelling the complex deformation histories of subglacial sediments (e.g. van der Meer 1987, 1993, 1996, 1997; Menzies & Maltman 1992; Seret 1993; Menzies 2000; Khatwa & Tulaczyk 2001; Hart & Rose 2001; Piotrowski *et al.* 2006; Larsen *et al.* 2006a, b; Phillips *et al.* 2007, 2012; Kilfeather *et al.* 2010; van der Meer & Menzies 2011; Menzies 2012); however, glacigenic sediments associated with the CIS have yet to be examined in detail at the microscale.

In the mid-1990s, macroscale field observations of Kamloops Lake till (till deposited during the maximum of the last, Fraser, glaciation) and bedrock in south-central BC, Canada were used to infer the thermal conditions that existed beneath the parts of the CIS that would have influenced local ice-flow dynamics (Lian 1997; Lian & Hicock 2000). The conclusions drawn from these studies were based on a limited data set
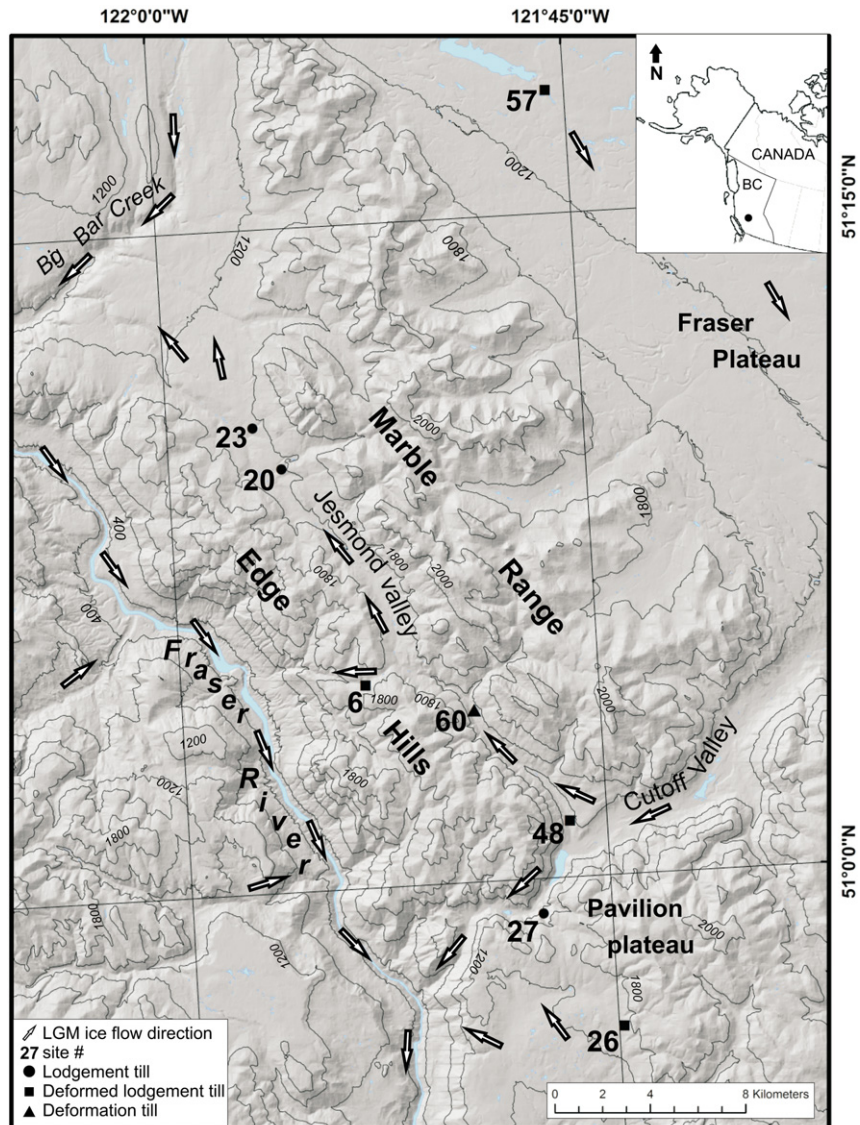
Fig. 1. The study area in British Columbia (BC), Canada. Site locations are superimposed on a hill-shaded and contoured (m a.s.l.) TRIM I digital elevation model (DEM) (Projection: Albers Conical Equal Area, Datum: NAD 83; Geobase ®). Last Glacial Maximum ice-flow directions and INQUA till classifications are based on Lian & Hicock (2000). This figure is available in colour at http://www.boreas.dk.

collected from a number of study sites between the Fraser River valley and the Fraser Plateau (Fig. 1). In this paper, we re-examine these deposits in more detail using both macroscale sedimentological and micromorphological observations. The research objectives of this study are twofold: (i) to use new field observations and qualitative micromorphological data in order to verify and refine previous interpretations of till genesis in the region, and (ii) to quantitatively analyse microstructure data using cluster analysis to see if the relative abundances of 'ductile'-type and 'brittle'-type microstructures in subglacial till reflect the previously proposed (Lian & Hicock 2000) till drainage conditions beneath the CIS. Here, we present the first integrated macroscale and micromorphological examination of subglacial till associated with the CIS.

Study area

Location and glacial history

The study area consists mainly of a small open-ended valley and an adjacent mountain plateau in south-central BC, Canada, which were informally referred to as Jesmond valley and Pavilion plateau, respectively, (Fig. 1) by Lian (1997); they flank the southwestern edge of the Fraser Plateau. All sites examined in this paper are situated within Jesmond valley, Cutoff Valley and on Pavilion plateau, except for Site 57, which is located on the Fraser Plateau east of the Marble Range (Fig. 1). Sites 25 and 26 of Lian & Hicock (2000) share the same traceable till unit (unit 2 of Neudorf 2008), and therefore are both referred to as Site 26 in this paper (Fig. 1).

During the onset of the Fraser Glaciation, ice advanced from the eastern and western mountain systems onto the interior plateaus of south-central BC (Clague *et al.* 1989; Clague & James 2002). At glacial maximum, the CIS is thought to have consisted of localised ice divides, domes, saddles and coalescent glaciers obtaining a maximum thickness of over 2000 m over major valleys, and several hundred metres over inland plateaus (Tipper 1971; Clague *et al.* 1989; Clague & James 2002). Glaciotectonic structures and clast fabrics measured from till deposited during the Fraser Glaciation (Kamloops Lake till; Fulton & Smith (1978); cf. Lian & Hicock (2001)) in the study area suggest that early ice spilled into the northern end of the Jesmond valley from the Fraser Plateau, and into the southern end of Jesmond valley from Cutoff Valley (Lian & Hicock 2000). Till clast fabrics, supported by the orientation of glaciotectonic structures in till and subtill sediments and bedrock, suggest that during the Last Glacial Maximum (LGM), the dominant ice-flow direction in Jesmond valley and on Pavilion plateau was from the SE (Fig. 1) (Lian & Hicock 2000). Bedrock striae, glacial grooves and streamlined landforms suggest that at the LGM, ice flow in the Fraser River valley and on Fraser Plateau was from the NW (Fig. 1) (Lian & Hicock 2000; Plouffe *et al.* 2009, 2011).

Kamloops Lake till has been studied at several sites and inferred to record a range of subglacial conditions ranging from wet and warm to dry and cold (Lian 1997; Lian & Hicock 2000). The style of till deposition was influenced largely by topography and substrate permeability (Lian & Hicock 2000; Plouffe *et al.* 2011). Under better-drained conditions in open areas, such as at the northern end of Jesmond valley or on the plateaus (e.g. sites 20, 23, 57 and 26, Fig. 1) till deposition at glacial maximum was thought to have occurred mainly through lodgement processes, with minimal postdepositional glacigenic reworking (Lian & Hicock 2000). Well-drained conditions were inferred from till units containing fissility, and tension and shear fractures with little, or no evidence of ductile deformation. Ploughing and lodging processes were inferred from pebbles in the till matrix showing strong alignment in the direction of ice flow, similarly oriented clast surface striae, facets on clast tops, *in situ* boat-shaped bottoms or 'keels', smooth, striated stoss sides (referred to here as 'stoss ends'), and rough or plucked lee sides (referred to here as 'lee ends') that were, for the most part, consistently oriented (cf. Krüger 1984; Benn 1995; Hart 2006b). However, the ice-flow history inferred for Jesmond valley is complex: at the north end of Jesmond valley ice flow during advance was southwards, whereas it was northwards as ice thickened during the LGM (Lian & Hicock 2000). This complex ice-flow history may have resulted in a switch in bed drainage conditions from poorly drained (ice advancing up an adverse slope) to well drained (LGM ice flow down a negative slope) during the Fraser Glaciation, although no macroscale record of poorly drained conditions has been previously reported at the northern end of Jesmond valley (Lian & Hicock 2000).

Where drainage was poor, such as in the confined southern part of Jesmond valley where the subglacial slope was adverse to the ice-flow direction at the LGM (e.g. Site 60, Fig. 1), pore-water pressure in the till matrix was thought to have increased as sedimentation proceeded, leading to a decrease in shear strength and subsequent ductile deformation under the shear stress of the overriding ice (Lian & Hicock 2000). Evidence for ductile deformation of the till matrix included preserved soft sandstone clasts that were eroded from the underlying bedrock and subsequently entrained by ductilely deforming till, variable pebble a-axis orientations (or spread fabric modes) (cf. Hicock & Dreimanis 1992; Hicock *et al.* 1996), and variable orientations of clast surface wear features such as striae and lee ends (cf. Hicock & Fuller 1995; Lian & Hicock 2000).

Till classification

Subglacial tills examined in south-central BC were classified as lodgement, deformed lodgement or deformation tills by Lian (1997) and Lian & Hicock (2000) using the criteria and definitions of the final report of the International Union for Quaternary Research (INQUA) Commission on Lithology and Genesis of Glacial Deposits, as reported by Dreimanis (1989). It should be noted that recent publications have proposed a complete revamping of the traditional till classification scheme to acknowledge that most subglacial tills are hybrids formed in a spatially and temporally dynamic subglacial environment where till deposition and deformation processes are virtually inseparable in the geological record (van der Meer *et al.* 2003; Piotrowski *et al.* 2004; Evans *et al.* 2006). Evans *et al.* (2006) are convinced that glacial geologists can confidently differentiate only between glaciotectonites (Benn & Evans 1998) and subglacial traction till (Evans *et al.* 2006). In their classification scheme, subglacial traction till encompasses the previously defined lodgement, deformed lodgement and deformation tills. This level of classification should be adhered to if only lithofacies and stone a-axis fabrics are analysed.

van der Meer *et al.* (2003) and Menzies *et al.* (2006) have suggested, on the basis of observations of till matrix micromorphology, that lodgement and melt-out tills *senso stricto* are not preserved at all in the geological record, and that all primary tills are products of a subglacial deforming bed (van der Meer *et al.* 2003; Menzies *et al.* 2006; Menzies 2012). They note that at the microscale, subglacial diamictons are dominated by deformation structures, and primary (or depositional) structures are rare. They have proposed the term

'tectomict' to describe all subglacial tills because they are the products of structural, tectonic (kinetic) processes as opposed to depositional processes (van der Meer *et al.* 2003), and may be differentiated from other diamictons (i.e. subaerial debris flows) according to the presence or absence of certain microstructures (Menzies *et al.* 2006). In BC, till lithofacies, macrofabrics and other data have been used together to classify lodgement till as that which formed when stones and debris at the base of moving ice ploughed into the substrate (Lian & Hicock 2000, 2010; Lian *et al.* 2003). As friction increased, they eventually detached from the ice and became lodged (Lian & Hicock 2000, 2010); this is the traditional definition of lodgement till (e.g. Boulton 1975; Dreimanis 1989). As the glacier continued to advance, the lodgement till thickened and/or the till experienced episodes of glaciotectonic deformation that overprinted the initial lodgement-type sedimentological characteristics. Till classified as deformed lodgement till showed evidence of post-lodgement deformation. Till classified as deformation till was thought to have been formed by glacially induced shear of subtill material (Elson 1989; Lian *et al.* 2003). Using these definitions, a lodgement till can turn into a deformation till if it deforms under an advancing glacier and new sediment is introduced into the unit as a result of shear (Lian & Hicock 2000, 2010; Lian *et al.* 2003).

In this paper, new macroscale and microscale sedimentological data from eight sites previously examined by Lian (1997) and reported by Lian & Hicock (2000) and Lian *et al.* (2003) are presented. The till at sites in the northern part of Jesmond valley and in Cutoff Valley was previously classified as mainly lodgement till. The till at Site 60 was classified as mainly deformation till. The till at all other sites was classified as deformed lodgement till (Fig. 1).

Methods

Macroscale sedimentology and structural geology

In the summer of 2006, macroscale observations and measurements were made from Kamloops Lake till at the sites shown in Fig. 1 to add to the data set produced by Lian (1997) and Lian & Hicock (2000). In addition, because some till exposures may have experienced significant erosion over the past decade, it was necessary to check that the sedimentological characteristics of any newly exposed till were consistent with observations made in the past. The sites in Fig. 1 were chosen so that subglacial processes beneath the CIS in locations that may be expected to be poorly drained (i.e. within topographically constricted areas – Jesmond valley, a tributary valley to the Jesmond valley in the Edge Hills, and Cutoff Valley, and valleys with slopes adverse to the ice-flow direction – the southern end of Jesmond valley

during the LGM) could be compared with those expected to be better drained (i.e. the topographically unconfined Fraser and Pavilion plateaus) (Fig. 1). Sites at the northern end of Jesmond valley may have experienced poorly drained conditions during glacial advance (ice flow was inferred to be SW up an adverse slope) but well-drained conditions during the LGM (ice flow to the NW down a negative slope; Fig. 1).

Macroscale observations included an assessment of till texture and macroscale deformation structures both in the till and in the underlying substrate, the nature of unit lower contacts (i.e. gradational versus sharp), the presence (or absence) and orientation (or trend) of glacigenic wear features on pebbles (see below), and the strength, shape and orientation of pebble a-axis fabrics (or macrofabrics). Macrofabric collection and analysis followed the protocol of Lian & Hicock (2000), whereby measurements are restricted to pebble-sized stones (with a maximum b-axis of about 6 cm) with a:b axis ratios of 2:1 to 3:2 and a minimum a- (long-) axis length of 1 cm. Pebble trend and plunge were plotted on lower-hemisphere Schmidt projections both as points and as contoured data (Fig. 2). Macrofabric modes were visually separated and tested against a random distribution at the 95% confidence level using the method of Woodcock & Naylor (1983) (cf. Hicock *et al.* 1996; Lian & Hicock 2000, 2010). Measurements that lie outside primary or secondary modes and are not statistically significant at the 95% confidence level are not included in the modal statistics and are considered outliers (cf. Lian & Hicock 2000). Primary and secondary mode principal eigenvectors are labelled 'M1' and 'M2', respectively. Macrofabric data are contoured at 1, 2, 3, etc. points per 100/N% of the projected area, where N is the number of measurements (Starkey 1977) (Fig. 2).

All pebbles measured for macrofabric analysis (50–60 pebbles in a sample) were examined for surface-wear features consistent with lodgement processes (cf. Lian & Hicock 2000, 2010). To avoid personal bias, clast macrofabric and surface-wear data were collected by at least two operators, with each operator collecting at least one macrofabric data set within a single till unit at a site. Glacigenic wear features on stone surfaces recorded in the field included the orientation of the youngest (or faintest) striae on pebble tops, the direction of stoss and lee ends, and the presence or absence of facets and keels. Symbols were added to each macrofabric stereogram to show the direction of stoss and lee ends, and the orientation of pebble surface striae (Fig. 2). The orientations of planar structures (strike and dip measured using a compass) in the till and underlying sediments or bedrock are plotted on the stereograms as poles to planes (Fig. 2). Particle size analysis (clay to very coarse sand; Wentworth 1922) was conducted on the matrix from each till sample using a Mastersizer 2000 (version 5.22) particle size analyser.
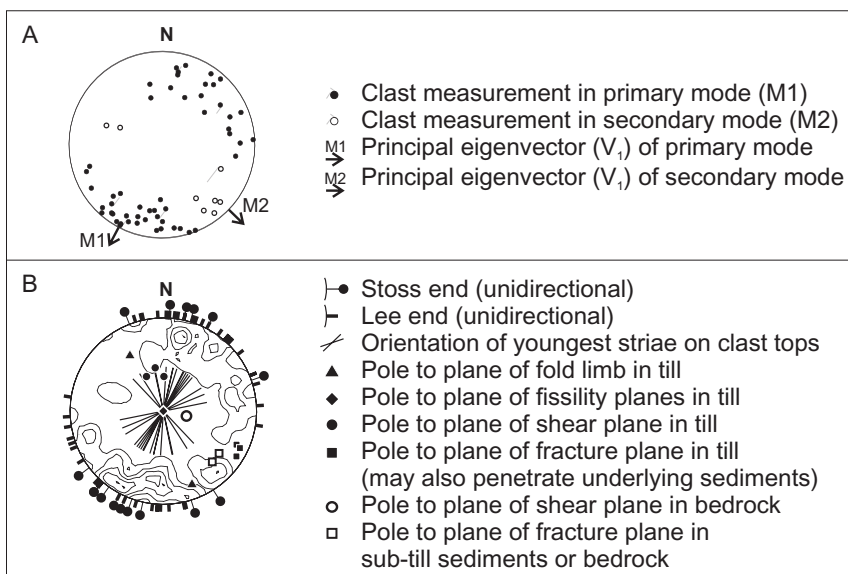
Fig. 2. Legend for macrofabric (pebble fabric) scatterplots (A) and contoured stereograms, including symbols for clast wear features, folds, fissility planes, shear planes and fracture planes (B). The principal eigenvectors in (A) point in the direction of maximum clustering within each mode. Measurements that do not fall inside a statistically significant mode are considered to be outliers. Pebble fabric data in (B) are contoured at 1, 2, 3, etc. points per 100/N% of the projected area, where N is the number of measurements (Starkey 1977).

Thin section preparation and micromorphological analysis

At all of the study sites, till was sampled for micromorphological analyses at one or more macrofabric sampling location. Owing to the highly consolidated and stone-rich nature of the till in this region, traditional sample extraction methods using Kubiena tins (e.g. van der Meer 1996) were impractical, and larger bulk sample blocks had to be carved out of the face with a pick axe. Before removing each sample block from the section face, the top and sides were coated with plaster of Paris and left to dry for 20 minutes. The top of each sample block was then shaved with a trowel and tested with a bubble-level to create a horizontal surface onto which the compass orientation of the sample block was marked. Each sample block was then extracted from the exposure and transported in a rigid container lined in bubble wrap to the Micromorphology Laboratory at Brock University, St. Catherines, Ontario, where it was impregnated with resin and thin sectioned using the protocol of Lee & Kemp (1992), Carr & Lee (1998) and van der Meer & Menzies (2006). Vertically oriented 5.0 × 7.5 cm^2 thin sections were prepared from all samples. The strike of each thin section face was intended to follow the direction of the macrofabric principal eigenvector, but, owing to a compass calibration error in the field, the strikes of all but one thin section are ~35°W of this. The strike of the vertical thin section from Site 27 was not recorded.

Micromorphological analysis included a qualitative assessment of microscale features as well as quantitative analysis of a subset of discrete microstructure types. Till microstructures were examined in all thin sections (18 thin sections in total) (e.g. Fig. 3A). Microstructures were identified at 10–40× magnification using a Leica M420 binocular polarising microscope and mapped (e.g. Fig. 3B). Skeletal grain lithology and shape, void type, relative abundance and pattern, and the extent of neoformation development were recorded and tabulated following the approach of Kilfeather & van der Meer (2008). The apparent long-axes of all visible sand and granule-sized grains were digitised from high-resolution (2400 dpi) scans of each thin section (e.g. Fig. 3C, D). This allowed the delineation of microfabric domains in which elongate grains share a similar preferred orientation, following the approach of Phillips et al. (2011) (e.g. Fig. 3C). Microfabric domains were mapped in order to illustrate the strain pattern of the till matrix, to identify multiple generations of microfabric development that may record multiple phases of till deformation (cf. Phillips et al. 2011), and to help explain the genesis of planar voids that may be fracture or shear planes. Phillips et al. (2011) proposed the use of a series of rose diagrams from different parts of a thin section in order to graphically display spatial variations in microfabric. Here, one rose diagram is used to summarize the microfabric of the entire area of each thin section, and spatial variations in microfabrics are enhanced by colour-coding the digitised grain long-axes according to their orientation using geographic information systems software (e.g. Fig. 3D).

A preliminary taxonomy of microfabrics and microstructures within glacial sediments was introduced by Menzies (2000: fig. 2). We find that most of these microstructure types (e.g. foliation, kink bands, faults, discrete shear lines, faulted domains, comet structures, sill and dyke structures, water escape structures, tiled units of laminated silts and clays and cutans) were rare or absent in our samples, or could not be identified with confidence owing to problems of
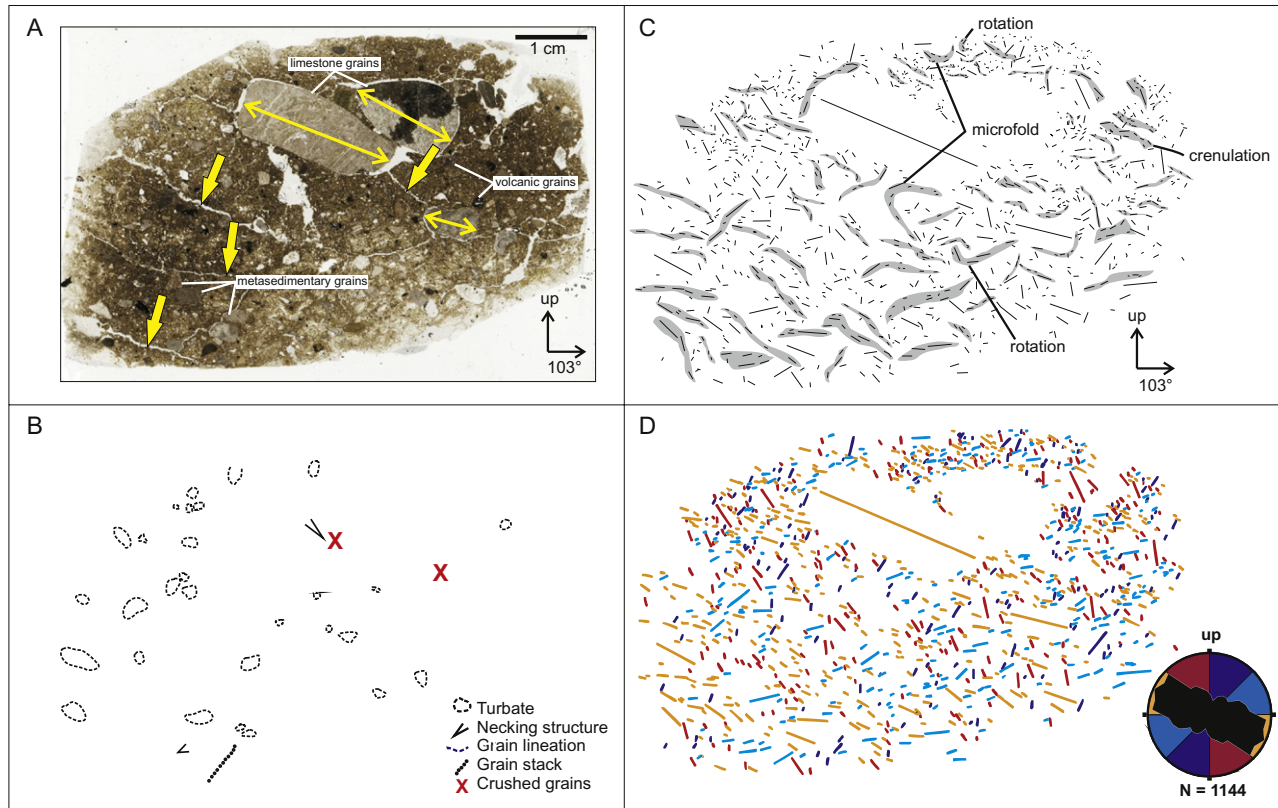
Fig. 3. Microphotograph (A) and microstructure map (B) of thin section S20F7 from Site 20. The yellow unidirectional arrows in (A) point to planar voids that are interpreted to be fissility planes. The yellow bidirectional arrows in (A) show the orientation of the long-axis of large skeletal grains. The black box in (A) delineates the total thin section area. Microfabric domains are highlighted in (C). In (D), grain orientations are colour-coded according to their orientation, and the four orientation classes are shown in the rose diagram. Grain long-axes that are coloured dark red or dark blue are oriented within 45° of the vertical plane, and those coloured light blue or orange are oriented within 45° of the horizontal plane. The majority of grains have a gentle apparent plunge down to 103° azimuth.

subjectivity. The apparent absence of kink bands, tiled units of laminated silts and clays and cutans is probably due to the low clay content (<30%) of our samples.

The classification and interpretation of microstructures is a subjective exercise, and few studies have made efforts to overcome problems of subjectivity (e.g. Zaniewski & van der Meer 2005; Larsen *et al*. 2007; Reinardy *et al*. 2011; Linch & van der Meer 2012). In this study, only microstructures that were composed of particular arrangements of skeletal grains, such as turbates, necking structures, grain lineations, grain stacks and crushed grains (Hooke & Iverson 1995; Menzies 2000; Hiemstra & Rijsdijk 2003; Larsen *et al*. 2006a, 2007), could be identified with confidence. Therefore, subjectivity was minimized by restricting our observations to discrete microstructures that were easily identifiable using a set of strict criteria outlined in Table 1. Turbates and necking structures are considered here to be 'ductile'-type microstructures that record episodes of ductile deformation of till with elevated pore-water pressure, whereas grain lineations, grain stacks and crushed/broken grains are considered to be 'brittle'-

type microstructures that record episodes of brittle deformation of till with relatively low pore-water pressure (Hooke & Iverson 1995; Menzies 2000).
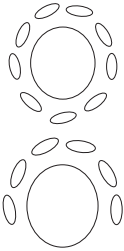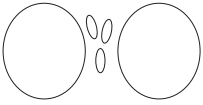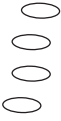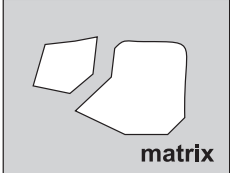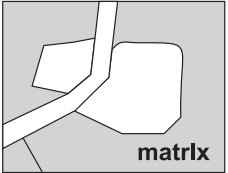
Plasmic fabrics (van der Meer 1993; Linch & van der Meer 2012) were not described or classified in this study because birefringent clays either were not observed (in all thin sections except for those from Site 26) or were too faint to classify with confidence (thin sections from Site 26). In Jesmond valley, the lack of visible plasmic fabrics in the till matrices sampled can be attributed to the high carbonate contents of the till matrix (11–18%, Lian 1997: table II.3), because carbonates are known to mask clay birefringence (van der Meer 1987). The lack of birefringent clay in the till at Site 57 on the Fraser Plateau is probably due to its low clay content, which is less than 1%.

Results

General macroscale observations

At the macroscale, Kamloops Lake till is typically homogeneous in colour (usually ranging from brown to

Table 1. Criteria for the identification of discrete microstructures.

Microstructure	Criteria[1]	Accepted	Not accepted
Turbates	Turbates were identified based on the circular arrangement of skeletal grains (cf. van der Meer 1993; Larsen *et al.* 2007). The majority of elongate grains of a similar size must be subparallel to the edges of the core stone on a minimum of 3 out of 4 sides. Turbate structures without core stones were rarely observed, but those that were counted consisted of encircling grains, with inter-particle distances smaller than the dimensions of the particles along the path of the circle.		
Necking structures	Includes preferred alignment of small grains between two adjacent large grains (sizes are relative) (cf. Larsen *et al.* 2006a). Counted necking structures did not include aligned particles that were part of turbates.		
Grain lineations	Identified by a minimum of three elongate grains aligned end-to-end (cf. Hiemstra & Rijsdijk 2003; Larsen *et al.* 2007). The distance between grains must be less than their lengths along the path of the lineation.		
Grain stacks	Includes a series of a minimum of four grains forming a subvertical stack (cf. Larsen *et al.* 2007). Only the flat edges (as opposed to corners) of the grains face each other. The distances between these grains must be smaller than their 'along-path' dimensions.		
Crushed or broken grains	Evidence of crushing or breakage must include separate pieces of the same grain suspended in the matrix (cf. Larsen *et al.* 2007). Pieces of a broken grain on either side of a fracture in the matrix were not included to avoid counting grains that may have been fractured during thin section grinding.	matrix	matrlx fracture in matrix

[1]Owing to the lack of birefringent clays and the clast-rich nature of the till, microstructure identification relied primarily on skeletal grain arrangements. Plasmic fabrics (e.g. Brewer 1976; Hiemstra & Rijsdijk 2003; Thomason & Iverson 2006) were not used to identify microstructures. See text for details.

grey) and in texture (Fig. 4). The till in the northern part of Jesmond valley (sites 20 and 23) and on the Fraser Plateau (Site 57) tends to be sandier than the till in the southern part of Jesmond valley (sites 6, 60 and 48), in Cutoff Valley (Site 27) and on the Pavilion plateau (Site 26). In most cases, the till is massive and the matrix is composed of sandy silt or silty sand with a minor clay component (Fig. 4). Till clast concentration was visually estimated and ranges from ~10 to ~40%.

Macrofabrics collected during this study, and in the previous study, are shown in Fig. 5 and are discussed in more detail in the following sections. At all sites, macrofabrics were measured in approximately the same locations within the till exposures as those reported in earlier studies (Lian 1997; Lian & Hicock 2000); however, some erosion of the exposures over the last decade was noted. Macrofabrics measured in this study
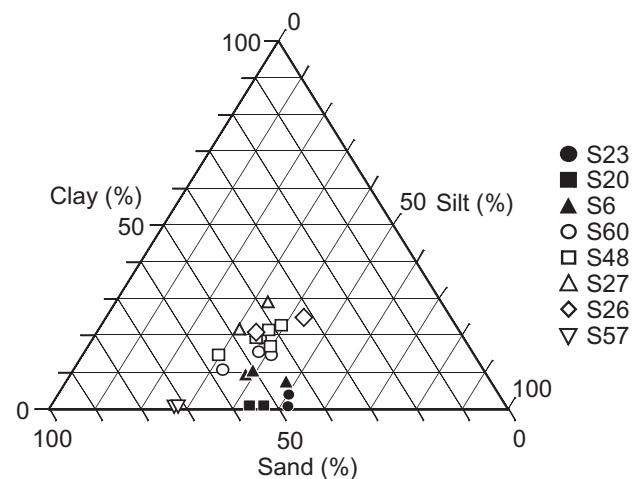

Fig. 4. Glacigenic diamicton matrix texture for all sites (2 to 5 samples were collected from each site).

Site #	Scatterplots and stereograms from previous studies	Scatterplots and stereograms from this study	
23	**F23** N=35, spread unimodal with outliers M1 eigenstatistics: $V_1=222°/9°$, $S_1=0.81$	**F30** N=61, spread bimodal M1 eigenstatistics: $V_1=208°/2°$, $S_1=0.68$ M2 eigenstatistics: $V_1=134°/12°$, $S_1=0.75$ Full sample eigenstatistics: $V_1=204°/4°$, $S_1=0.61$	**F31** N=59, spread unimodal with outliers M1 eigenstatistics: $V_1=222°/5°$, $S_1=0.83$ Full sample eigenstatistics: $V_1=222°/5°$, $S_1=0.78$
20	**F20** N=50, spread unimodal with outliers M1 eigenstatistics: $V_1=332°/5°$, $S_1=0.77$	**F7** N=60, spread unimodal M1 eigenstatistics: $V_1=321°/9°$, $S_1=0.80$	
6	**F6** N=32, spread unimodal with outliers M1 eigenstatistics: $V_1=241°/3°$, $S_1=0.75$	**F26** N=60, unimodal with outliers M1 eigenstatistics: $V_1=246°/7°$, $S_1=0.87$ Full sample eigenstatistics: $V_1=246°/7°$, $S_1=0.83$ **F33** N=60, spread bimodal M1 eigenstatistics: $V_1=58°/3°$, $S_1=0.75$ M2 eigenstatistics: $V_1=317°/4°$, $S_1=0.65$ Full sample eigenstatistics: $V_1=60°/4°$, $S_1=0.66$	**F27** N=60, spread bimodal M1 eigenstatistics: $V_1=245°/8°$, $S_1=0.75$ M2 eigenstatistics: $V_1=143°/17°$, $S_1=0.67$ Full sample eigenstatistics: $V_1=246°/9°$, $S_1=0.67$
60	**F60a** N=30, unimodal with outliers M1 eigenstatistics: $V_1=208°/12°$, $S_1=0.85$	**F11** N=60, spread bimodal M1 eigenstatistics: $V_1=59°/8°$, $S_1=0.57$ M2 eigenstatistics: $V_1=143°/32°$, $S_1=0.85$ Full sample eigenstatistics: $V_1=63°/10°$, $S_1=0.50$ **F13** N=60, spread unimodal M1 eigenstatistics: $V_1=212°/4°$, $S_1=0.55$	**F15** N=60, girdle-like M1 eigenstatistics: $V_1=22°/1°$, $S_1=0.42$ **F14** N=60, spread bimodal M1 eigenstatistics: $V_1=245°/9°$, $S_1=0.74$ M2 eigenstatistics: $V_1=331°/4°$, $S_1=0.74$ Full sample eigenstatistics: $V_1=209°/10°$, $S_1=0.59$

Fig. 5. Macrofabric scatterplots and stereograms for all tills examined in this study. F(number) refers to the macrofabric number. Refer to Fig. 1 for site locations and to Fig. 2 for the stereogram legend. Scatterplots and stereograms from previous studies (column 1) are from Lian (1997) and Lian & Hicock (2000). The macrofabric data are shown both as scatterplots (left) and as contour plots (right). Eigenstatistics are shown for both primary (M1) and secondary (M2) macrofabric modes. V_1 and S_1 are the principal eigenvector (reported as trend/plunge) and eigenvalue, respectively.

The figure contains a grid of stereonet fabric plots with the following labels and eigenstatistics:

Row 48:

F48 — N=50, girdle-like
M1 eigenstatistics: V_1=220°/14°, S_1=0.60

F9 — N=60, spread bimodal
M1 eigenstatistics: V_1=114°/15°, S_1=0.73
M2 eigenstatistics: V_1=37°/1°, S_1=0.69
Full sample eigenstatistics: V_1=101°/14°, S_1=0.52

F10 — N=60, girdle-like
M1 eigenstatistics: V_1=73°/29°, S_1=0.43

F17 — N=60, bimodal
M1 eigenstatistics: V_1=235°/6°, S_1=0.81
M2 eigenstatistics: V_1=328°/6°, S_1=0.77
Full sample eigenstatistics: V_1=234°/5°, S_1=0.70

F32 — N=60, spread bimodal
M1 eigenstatistics: V_1=217°/2°, S_1=0.69
M2 eigenstatistics: V_1=317°/3°, S_1=0.74
Full sample eigenstatistics: V_1=214°/2°, S_1=0.60

Row 27:

F27 — N=60, spread unimodal with outliers
M1 eigenstatistics: V_1=211°/5°, S_1=0.88

F2 — N=60, spread unimodal
M1 eigenstatistics: V_1=199°/6°, S_1=0.73

Row 26:

F26a — N=50, spread bimodal
M1 eigenstatistics: V_1=280°/24°, S_1=0.76
M2 eigenstatistics: V_1=359°/11°, S_1=0.88

F28 — N=60, girdle-like
M1 eigenstatistics: V_1=272°/24°, S_1=0.48

F29 — N=60, spread bimodal
M1 eigenstatistics: V_1=273°/16°, S_1=0.72
M2 eigenstatistics: V_1=197°/10°, S_1=0.68
Full sample eigenstatistics: V_1=270°/15°, S_1=0.63

Row 57:

F57 — N=50, spread unimodal with outliers
M1 eigenstatistics: V_1=190°/3°, S_1=0.71

F19 — N=60, spread bimodal
M1 eigenstatistics: V_1=173°/1°, S_1=0.71
M2 eigenstatistics: V_1=280°/7°, S_1=0.69
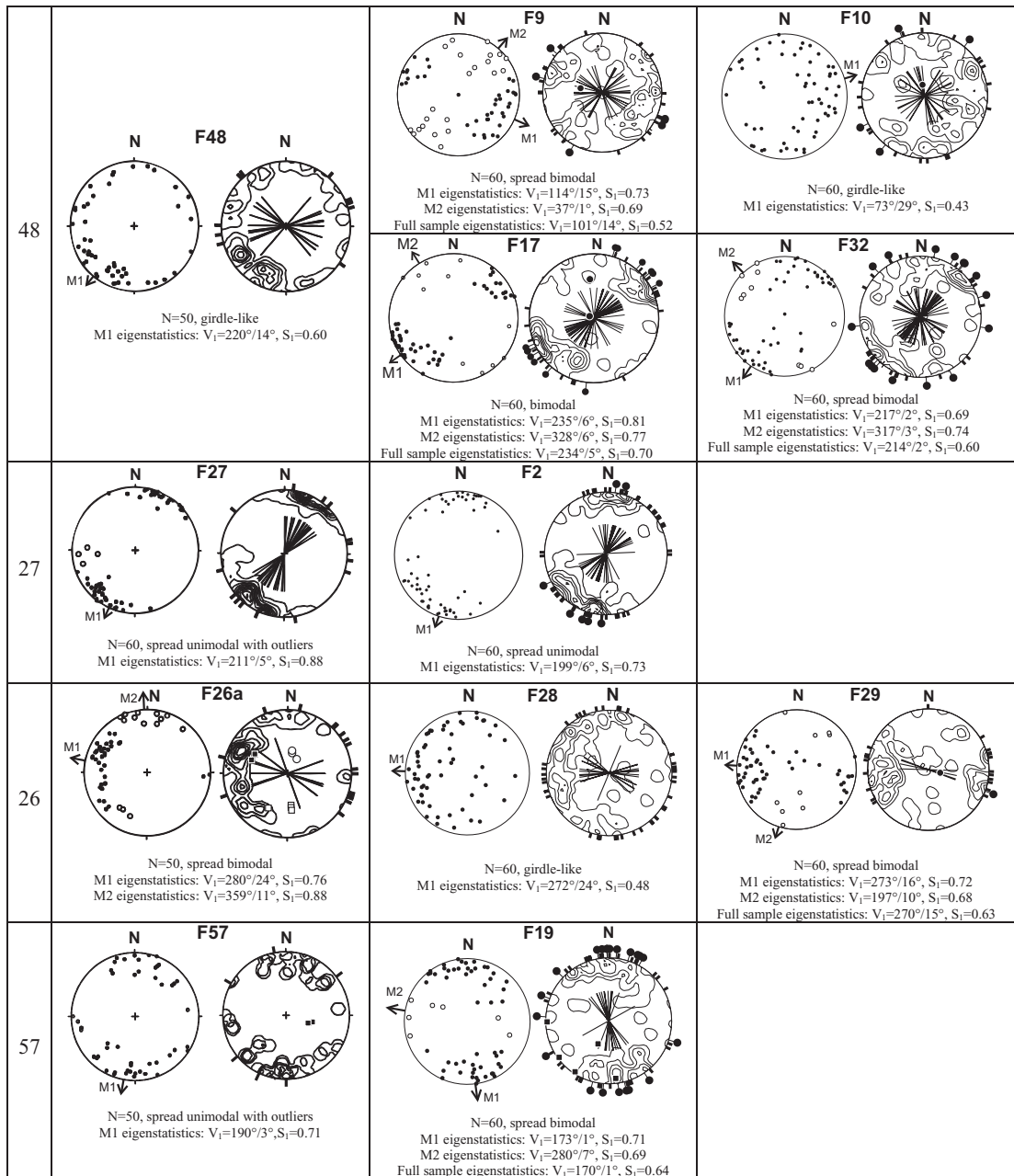Full sample eigenstatistics: V_1=170°/1°, S_1=0.64

Fig. 5. Continued

are generally consistent with those reported by Lian & Hicock (2000) (Fig. 5), and thus add directly to those data sets. At each of five sites, two to four macrofabrics were measured (Fig. 5). Macrofabrics recorded at sites 48 and 60 show lateral variation, but those measured closest to Lian's (1997) macrofabrics F60a (F14, this study) and F48 (F32, this study) are consistent with past observations (Lian 1997; Lian & Hicock 2000) (Fig. 5). Some of the macrofabrics measured at sites 23, 6, and 60 show additional modes not present in Lian's (1997) data (e.g. macrofabrics F30, F27 and F33, Fig. 5). This probably reflects the larger number of pebbles measured in this study (e.g. 35 pebbles at Lian's macrofabric F23 versus 61 pebbles at macrofabric F30 in this study; Fig. 5).

Pebble lithologies in the till are typically representative of the local bedrock, which consists mainly of limestone (the Marble Range), chert, argillite, siltstone, andesite (Pavilion plateau and the Edge Hills) and basalt (Pavilion plateau, the Edge Hills and the Fraser Plateau) (Fig. 1) (Roddick *et al.* 1979). All till exposures examined in this study have significant numbers of clasts with glacigenic wear features, including stoss and lee ends and facets, and these are best preserved on

large pebbles, cobbles and boulders of argillitic or limestone lithologies. Stone keels were difficult to identify and/or are rare and therefore are not included in subsequent analyses in this paper. Striae on the upper surfaces of clasts are usually aligned with clast a-axes, and pebble stoss and lee features do not show a preferred direction in till investigated at most sites (Fig. 5).

General microscale observations

Thin sections of the till at most sites in the study area show a homogenous, poorly sorted matrix (e.g. Site 20, Fig. 3A), although some have unique characteristics. For example, thin sections from the poorly consolidated till at Site 26 show a heavily fractured matrix, and the till at Site 27 shows discrete domains of different colours that probably correspond to the brown and grey components of the till observed at the macroscale.

Void and neoformation types and their relative abundances in all thin sections are summarized in Table 2. All thin sections have vesicles and vughs, and these are particularly visible in areas where uneven hand-grinding has reduced the thin section thickness. Planar voids appear at most sites and are typically randomly oriented, or related to fissility planes (Table 2). Neoformations commonly occur as $CaCO_3$, Fe or Mn precipitate that stains the matrix, or coats void walls and/or grains (Table 2). In the following sections, the till architecture, macroscale sedimentary structures, macrofabrics and micromorphology at each study site are summarised and interpreted. Microphotographs, microstructure maps and microfabric diagrams for till at sites 23, 6, 60, 48, 27, 26 and 57 are included in the Supporting Information for this article (Figs S1–S17).

Individual site descriptions

Northern Jesmond valley macroscale observations. – In the northern part of the Jesmond valley, subhorizontal fissility planes or silt-filled fracture and shear planes are observed in till at two sites (sites 20, 23; Figs 1, 6A, B). These structures are mostly visible near the upper contact of the till, where calcium carbonate has precipitated from groundwater and/or meteoric water along fracture plane walls. Fissility planes in the till at Site 23 gently dip down to the SE, and shear planes at Site 20 dip down to the WNW (Fig. 5).

The macrofabrics measured from till in the northern part of Jesmond valley are spread unimodal, or spread bimodal but with a dominant main mode. Macrofabrics F30 and F31 at Site 23 were taken ~45 m apart. Both macrofabrics have main modes oriented NE–SW. The main macrofabric mode at Site 20 is oriented NW–SE. This is subparallel to the orientation of Jesmond valley, and to the dips of a series of NW-dipping fractures measured by Lian & Hicock (2000) (Fig. 5).

Northern Jesmond valley micromorphology. – In thin section, the till at sites 20 and 23 is plasma-supported and dominated by subangular to subrounded limestone and metasedimentary grains followed by subrounded to rounded volcanic grains (Table 2; Figs 3A, S1A, S2A). The fissility planes observed at the macroscale are expressed as subparallel planar voids in thin section, and the apparent long-axes of some of the largest skeletal grains are oriented subparallel to these planes (Table 2; Figs 3A, S1A, S2A). The orientation of the planar voids is generally consistent with the orientation of most sand-sized grains and microfabric domains in thin sections S23F31 and S20F7 (Figs 3, S2) and a fraction of the grains (delineated in orange in Fig. S1B) in thin section S23F30. Microfabric domains are aligned with the edges of some skeletal grains and form microfolds and crenulations in all thin sections (Figs 3C, S1C, S2C). Discrete microstructures including turbates, necking structures and grain stacks are present in the till at both sites (Figs 3B, S1B, S2B). Grain lineations are absent at Site 20, and crushed grains are absent at Site 23 (Figs 3B, S1B, S2B).

Northern Jesmond valley interpretations. – The limestone, metasedimentary and volcanic grains observed in thin section are consistent with the geology of the bedrock along the length of the Jesmond valley, suggesting that the till is locally derived. Subhorizontal fissility planes observed at sites 20 and 23 (Fig. 5) probably record pervasive shearing of the till matrix (Broster *et al.* 1979; van der Meer *et al.* 2003), but may also record relaxation of the till matrix during unloading after retreat or melting of overriding glacial ice (Lian 1997) and/or postdepositional freeze–thaw action (van Vliet-Lanoë *et al.* 1984). The NW dip of most silt-filled shear planes in the till at Site 20 (Fig. 6B) is consistent with the general orientation of pebble a-axes, and the apparent dips of planar voids in thin section S20F7 are consistent with the long-axis orientation of many sand grains. Thus these planar voids may be shear planes that record shearing of the till underneath SE-flowing ice that advanced across an adverse slope in Jesmond valley before the LGM, as previously suggested by Lian & Hicock (2000). The planar voids observed in thin sections S23F30 and S23F31 may record shear or relaxation of the till matrix along planes consistent with the apparent orientation of microfabrics (highlighted in orange in Figs S1D and S2D) and microfabric domains. Microfolds, crenulations, turbates and necking structures in the till at sites 20 and 23 are suggestive of microscale ductile deformation (folding, kinking and squeeze-flow) and the plastering of matrix particles around skeletal grains. The grain lineations at Site 23, the crushed grains at Site 20, and the grain stacks observed at both sites are suggestive of brittle deformation and

Table 2. Micromorphological features, including the relative abundance of voids and neoformations.

Sample	Skeleton grains[1]		Matrix	Voids[2,3]						Neoformations		
	Lithology	Shape	Sorting/ structures	Relative quantity	Vesicle	Vugh	Planar voids associated with fissility	Systematic or cross-cutting planar voids	Randomly oriented planar voids	$CaCO_3$/Fe/Mn staining in matrix	Void coats	Grain coats
Northern Jesmond valley												
S20F7	L>MS>V	SA-R		○○	●	●	●			○($CaCO_3$; Fe or Mn)	○($CaCO_3$; Fe or Mn)	○($CaCO_3$)
S23F30	L>MS>V	SA-R		○○	●	●	●			○○($CaCO_3$)	○($CaCO_3$; Fe or Mn)	○○($CaCO_3$; Fe or Mn)
S23F31	L>MS>V	SA-R		○○○	●	●	●			○○($CaCO_3$; Fe or Mn)	○○($CaCO_3$;Fe or Mn)	○○($CaCO_3$; Fe or Mn)
Edge Hills												
S6F26	MS>L>V	A-R		○○	●	●	●			○($CaCO_3$)		○($CaCO_3$)
S6F27	MS>L>V	A-R		○○	●	●	●				○○○(Ca)	
S6F33	MS>L>V	A-R		○○○	●	●	●		●			
Southern Jesmond valley												
S60F11	L>MS>V	SA-R	sand inclusion	○	●	●			●			
S60F13	L>MS>V	SA-R		○○○	●	●			●●	○○($CaCO_3$)		○○($CaCO_3$)
S60F14	L>MS>V	SA-R		○○○	●	●			●	○○($CaCO_3$)		○○($CaCO_3$)
S60F15	L>MS>V	SA-R		○○○	●	●			●	○(Fe or Mn)		
S48F9	L>MS>V	SA-R		○○○	●	●	●?	●		○○(Fe or Mn)	○○(Fe or Mn)	○○(Fe or Mn)
S48F10	L>MS>V	SA-R		○○	●	●		●●		○○(Fe or Mn)	○○(Fe or Mn)	○○(Fe or Mn)
S48F17	L>MS>V	SA-R		○○	●	●				○○(Fe or Mn)	○○(Fe or Mn)	○○(Fe or Mn)
S48F32	L>MS>V	SA-R		○○	●	●		●●		○○(Fe or Mn)	○○(Fe or Mn)	○○(Fe or Mn)
Cutoff Valley												
S27F1	MS	SA-SR	mixing	○○	●	●			●			○(Fe or Mn)
Pavilion and Fraser plateaus												
S26F28	MS	SR		○○○	●	●		●		○○($CaCO_3$)	○(Fe or Mn)	
S26F29	MS	SA-SR		○○○	●	●				○○($CaCO_3$)	○(Fe or Mn)	
S57F19	V>>L	SR-R		○	●	●			●	○○(Fe or Mn)	○○(Fe or Mn)	○○(Fe or Mn)

[1]L = limestone; MS = metasedimentary (mostly argillite); V = volcanic (>,< indicate relative abundance); R = rounded; SR = subrounded; SA = subangular.

[2]○ = rare/poorly developed; ○○ = more common/better developed; ○○○ = frequently occurring/well developed.

[3]● = present; ●? = uncertainty about whether or not the planar voids are fissility planes.
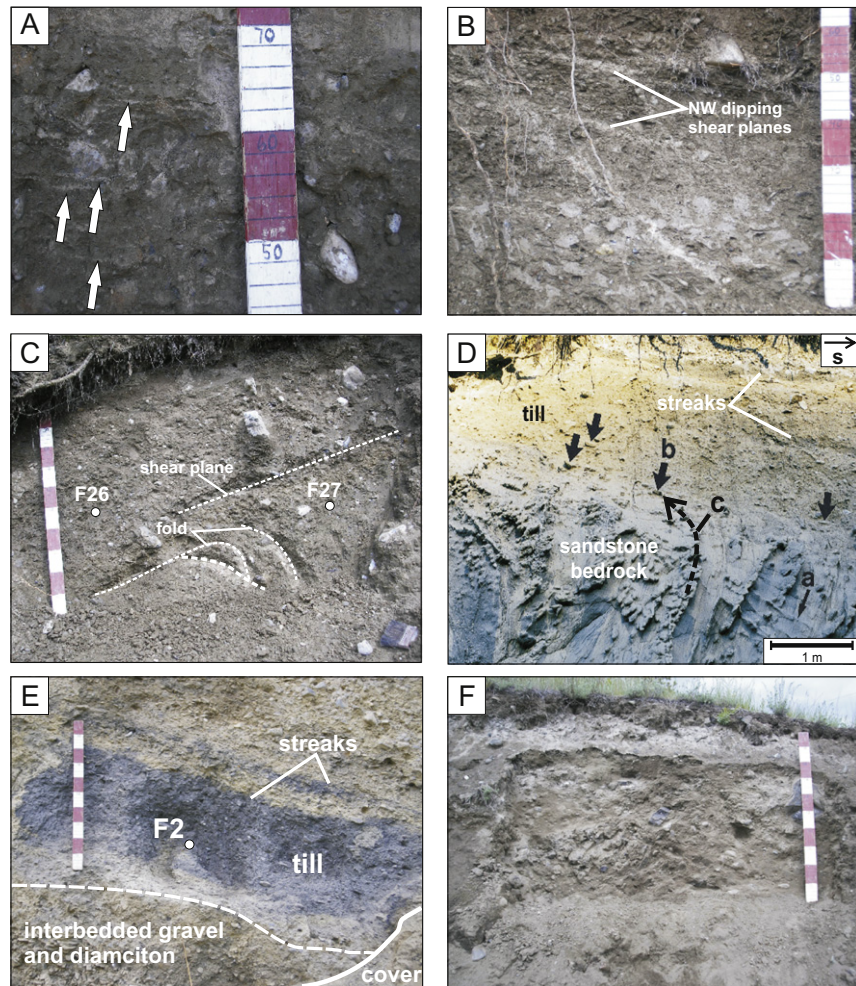
Fig. 6. A. Fissility planes (arrows) in the till matrix at Site 23. B. Silt-filled shear planes at Site 20. C. A fold and shear plane at Site 6. D. The erosive lower contact of the till at Site 60, exposure 1. Shear planes in the bedrock (A) dip to the SW. Angular blocks of sandstone (B) have been entrained into the base of the till unit, and the bedrock has been deformed near its upper contact (C). E. Dark grey streaks in otherwise massive till at Site 27. F. Massive till with limestone and basaltic clasts at Site 57. Metre stick with decimetre subdivisions for scale. This figure is available in colour at http://www.boreas.dk.

increased friction between sand grains under relatively low pore-water pressure (Hooke & Iverson 1995).

Edge Hills macroscale observations. – Site 6, located on the west side of the Edge Hills drainage divide in a tributary valley to Jesmond valley (Fig. 1), contains a fold underlying a shear plane within an otherwise structureless till matrix (Fig. 6C). The limbs of the fold near the vicinity of macrofabrics F26 and F27 dip to the NW and SE and are indicative of a NE–SW-trending fold axis that is oriented subparallel to the macrofabric main mode (Figs 5, 6C). The apparent dip of the shear plane is subparallel to the NW limb of the fold. Macrofabrics F26 and F27 were measured within a metre of each other (Fig. 6C), and macrofabric F33 was measured ~20 m east of F27. All macrofabrics at Site 6 show main macrofabric modes oriented subparallel to the NE–SW-trending tributary valley within which this till was deposited (Figs 1, 5). Macrofabrics F27 and F33 have NW–SE-trending transverse secondary modes (Fig. 5).

Edge Hills micromorphology. – In thin section, the till at Site 6 is plasma-supported and dominated by angular to subrounded metasedimentary skeletal grains (argillite grains often appear as elongate angular shards), with smaller amounts of subangular to rounded limestone grains and subrounded volcanic grains (Table 2; Figs S3A, S4A, S5A). Two of the three vertical thin sections (S6F26 and S6F33) contain subparallel planar voids, and these are subparallel to the orientation of most sand grains in S6F26 (Table 2; Fig. S4). Microfabric domains are aligned with the edges of some skeletal grains and form microfolds and crenulations in all thin sections (Figs S3C, S4C, S5C). Most curvilinear microfabric domains are similarly oriented in thin sections S6F26 and S6F27 (Figs S3C, S4C). In thin section S6F33, NNE-plunging microfabric domains (grey) are cross-cut by SSW-plunging microfabric domains (blue) (Fig. S5C). Discrete microstructures including turbates, necking structures, grain lineations, grain stacks, and crushed/broken grains are present in this till (Figs S3B, S4B, S5B).

Edge Hills interpretations. – Deformation in the form of a NW–SE compression and shear event is evident from the fold and overlying shear plane observed at Site 6.

This NW–SE compression could have occurred under ~W-flowing ice draining the Jesmond valley at the LGM (Fig. 1). Ductile deformation of the till beneath the shear plane may be responsible for the greater spread in pebble orientations in macrofabric F27 (below the shear plane) relative to macrofabric F26 (above the shear plane) (Fig. 6C). The apparent dip of the shear plane is parallel to the NW limb of the fold, which appears attenuated. The shear event probably post-dates the folding event, leading to attenuation of the NW limb of the fold. The relative paucity of limestone skeletal grains observed in thin section (Figs S3A, S4A, S5A) can be explained by the location of this till, which is in the Edge Hills ~2.5 km away from the limestone outcrops of the Marble Range (Fig. 1). Curvilinear microfabric domains, turbates and necking structures are indicative of ductile deformation of the till matrix at the microscale, while grain stacks and crushed grains are indicative of increased inter-grain friction and fracturing under low pore-water pressure (Hooke & Iverson 1995). The cross-cutting microfabric domain pattern observed in thin section S6F33 (Fig. S5C) may be the remnants of a previous (or subsequent) deformation event that formed a shear plane.

Southern Jesmond valley macroscale observations. – Till exposed at sites 60 and 48 in southern Jesmond valley is overlain by poorly sorted and weakly bedded pebble–cobble gravel and sand (Fig. 7A, B) that has previously been interpreted as having been deposited by streams during ice retreat (Lian 1997). The till at Site 60 is exposed along two roadcuts: one on the east side of Jesmond Road following the length of Jesmond valley (exposure 1, Fig. 6D), and one along a small access road less than 50 m NE and upslope of the first roadcut (exposure 2, Fig. 7A).

The till in exposure 1 has dark grey, subhorizontal streaks and a sharp lower contact. Angular fragments of the underlying semi-lithified and friable sedimentary bedrock (sandstone, siltstone and conglomerate) are aligned in an apparently curved arrangement (curved to the north) in the base of the till (Fig. 6D). Several subrounded to rounded bedrock clasts were observed a few metres above the lower contact of the till in exposure 2 (Figs 7A, 8). These also consist of semi-lithified, friable sedimentary rock but are more rounded than the sandstone fragments observed near the till/bedrock contact in exposure 1 (Fig. 6D). Shear planes in the bedrock immediately underlying the till measured by Lian & Hicock (2000) dip to the SW. The till in exposure 2 contains shear planes (Fig. 7A) that are either subhorizontal (around macrofabric F14, Fig. 5), or are gently dipping to the SW (around macrofabric F15, Fig. 5). A few fractures dipping to the NW and NE were measured near macrofabrics F11, F13 and F14 (Fig. 5). Several steeply dipping fractures extend from the till, through its lower contact and into an underly-

ing glaciofluvial sand unit that was interpreted to have been deposited during glacial advance (Lian 1997) and is NW of macrofabric F15 (Fig. 7A; F15, Fig. 5). The till at Site 48 has shear planes dipping gently to the SW (Fig. 7B; F17, F9, F10, Fig. 5). The lower contact of the till at Site 48 was not exposed, and similar soft sediment clasts were not observed.

Previously, only one macrofabric was measured from each of sites 60 and 48 (Lian & Hicock 2000). The macrofabric measured at Site 60 shows a NNE–SSW-trending mode and that at Site 48 shows pebbles with variable orientations (Fig. 5). Additional macrofabrics sampled at four different locations within the till unit at sites 60 (exposure 2) and 48 show lateral and vertical changes in modality and main mode orientations (Figs 5, 7A, B). Macrofabrics with spread unimodal or bimodal distributions have modes oriented either NE–SW (parallel to shear planes in the till and in the underlying bedrock, and to the local valley wall at exposure 1, Site 60) or NW–SE, parallel to the axis of Jesmond valley (Fig. 5).

Southern Jesmond valley micromorphology. – Like the till observed in the northern part of Jesmond valley, the till at sites 60 and 48 is dominated by subangular to subrounded limestone and metasedimentary grains followed by subrounded to rounded volcanic grains (Table 2; Figs S6–S13). In general, the diamicton appears plasma-supported, except for a sand inclusion on the left side of thin section S60F13 (Fig. S7A, B). At Site 60, planar voids show no systematic pattern or preferred orientation within any of the thin sections, and thin sections S60F14, S60F15 and S60F13 have larger, more frequent voids than S60F11 (Table 2; Figs S6–S9).

Three thin sections from Site 48 have systematically oriented (S48F17 and S48F32) or cross-cutting (S48F9) planar void patterns (Table 2; Figs S10A, S12A, S13A). Skeletal grain orientations and microfabrics do not seem to be influenced by fracture patterns in any of the thin sections in the southern part of Jesmond valley (Figs S6–S13; Table 2). Microfabric domains are typically randomly oriented. In thin section S60F14, one set plunges to the NNW (grey) and is crosscut by another set that plunges to the SSE (blue) (Fig. S8C). In thin section S48F17 they plunge steeply down to the NNE (Fig. S12). Turbates, necking structures, grain lineations, grain stacks and crushed/broken grains are common at both sites (Figs S6–S13).

Southern Jesmond valley interpretations. – At Site 60, episodes of ductile deformation of till probably resulted in the reorientation of pebbles, yielding spread bimodal to girdle-like macrofabric modes (cf. Hicock *et al.* 1996) and erosion and entrainment of the underlying bedrock (Lian & Hicock 2000). Bedrock (soft pebbly siltstone and sandstone) clasts in the till become more
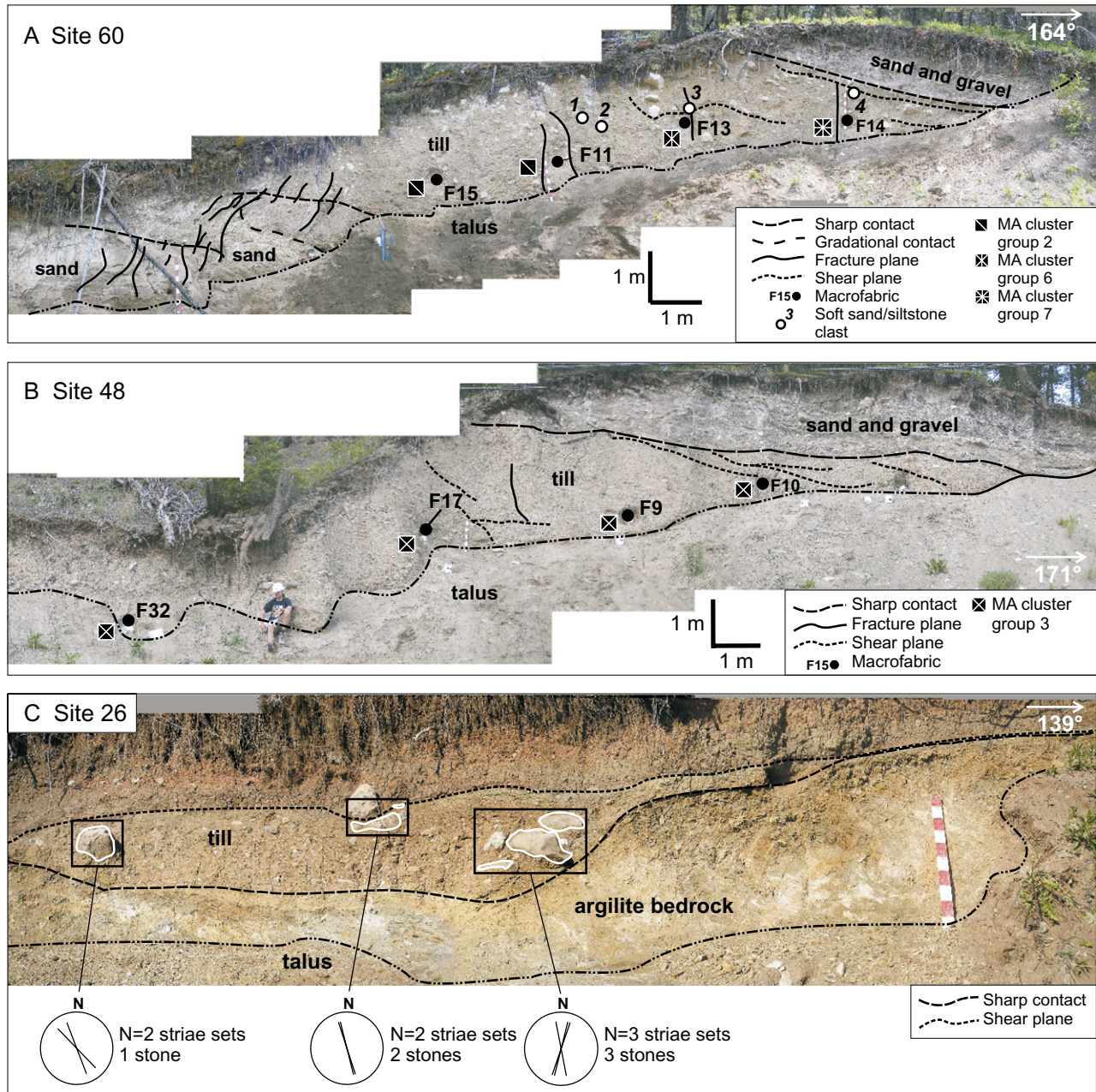
Fig. 7. Macrofabric locations and geological structures in till at Site 60, exposure 2 (A), Site 48 (B), and Site 26 (C). See Fig. 8 for photographs of sand/siltstone clasts 1–4 in (A). Microstructure association (MA) cluster groups for thin sections from sites 60 and 48 are shown in (A) and (B) (see text for explanation). At Site 26 (C), macrofabric F28 is measured in the diamicton ~20 m to the left edge of photograph, and macrofabric F29 is measured ~2 m to the right edge of the photograph. The orientations of striae sets on the tops of boulders at Site 26 are plotted on stereograms in (C). Metre stick with decimetre subdivisions for scale. This figure is available in colour at http://www.boreas.dk.

rounded with distance from the till–bedrock interface (exposure 1, Fig. 6D; exposure 2, Fig. 7A). This suggests that after entrainment into the till matrix, bedrock clasts behaved as rotational elements during periods of elevated pore-water pressure and became rounder with distance from their source as a result of surface abrasion (van der Meer 1997; Lian & Hicock 2000). The till

at Site 60 may have been susceptible to elevated pore-water pressures owing to poor drainage of the substrate on a slope that was adverse to the ice-flow direction at the LGM (Fig. 1). Evidence of brittle deformation is superimposed on the ductile deformation signature in the till at Site 60 in the form of SSW-dipping shear planes and generally north-dipping tension fractures in

Fig. 8. Indurated sediment clasts found in the till at Site 60 (see Fig. 7A for clast locations in exposure 2). Clasts 1 and 3 are composed of light yellow massive pebbly silt. Clast 2 is composed of laminated silt and sand, and clast 4 consists of inter-bedded partially oxidized sand and pebble-gravel. The head of the geologic hammer is 6 cm wide. The metre stick is painted with decimetre subdivisions. This figure is available in colour at http://www.boreas.dk.

the till (F15, Fig. 5). These record a later phase of brittle glaciotectonic deformation of a well-drained substrate under north-flowing ice (Lian & Hicock 2000). Preservation of the pebbly silt and sandstone bedrock clasts in the till suggests that episodes of brittle deformation of the substrate were confined largely to a shear zone of limited thickness immediately below the ice-bed interface (Piotrowski *et al.* 2001), or to relatively widely spaced glaciotectonic shear and fracture zones at depth within the till (Fig. 7A) (Truffer *et al.* 2000).

Spread bimodal and girdle-like macrofabrics are also present in the till at Site 48, a few kilometres SSE of Site 60. Independent macroscale evidence for ductile deformation of this deposit is lacking, so some or all of the spread in pebble orientations may be associated with local shifts in ice-flow direction (Lian & Hicock 2000). Site 48 is located near the junction of Cutoff and Jesmond valleys, where local shifts in ice-flow direction may have occurred as ice from Cutoff Valley drained ~north into Jesmond valley (Fig. 1). SE- and SSE-dipping shear planes in this till (Figs 5, 7B) may record the same episode of brittle deformation under north-flowing ice as that observed at Site 60.

Skeletal grain orientations and microfabrics do not seem to be influenced by planar void orientations in any of the thin sections from sites 60 and 48 (Table 2), suggesting that planar voids are probably fractures rather than shear planes. This inference is supported by the fact that planar voids in most thin sections (except for thin sections S48F9, S48F17 and S48F32) are randomly oriented (Table 2) rather than preferentially oriented in response to a unidirectional shear stress field

(cf. Hiemstra & Rijsdijk 2003; Menzies 2012). It is possible that these fractures formed during desiccation of the till after deposition, or perhaps during sampling and thin section preparation. Curvilinear microfabric domains, turbates and necking structures are indicative of ductile deformation of the till matrix at the microscale, whereas grain stacks and crushed grains are indicative of increased inter-grain friction and fracturing under relatively low pore-water pressure.

Cutoff Valley, macroscale observations. – Site 27 is located in the topographically constricted Cutoff Valley on a neutral slope (Fig. 1). The till is highly consolidated, overlies interbedded pebble–boulder gravel and diamicton, and contains dark grey bands close to and subparallel to its lower contact (Fig. 6E). The macrofabric is spread unimodal with a main mode oriented NE–SW (F2, Fig. 5).

Cutoff Valley micromorphology. – The till matrix in thin section S27F1 is a mixture of two diamictons of different colours: one dark grey and one brown (Fig. S14A). The dark grey diamicton in S27F1 forms jagged, semi-continuous patches of plasma with diffuse to sharp edges that appear dispersed throughout brown-coloured plasma (Fig. S14A). Many fractures in thin section S27F1 appear to follow paths restricted to the brown plasma, suggesting that the brown diamicton matrix is less cohesive (Fig. S14A). Turbates, grain lineations, necking structures and crushed grains occur in decreasing order of abundance (Fig. S14B). Two sets of microfabric domains (coloured grey and blue in Fig. S14C) cross-cut each other in thin section S27F1. The

orientation of the plane of this vertically oriented thin section was not measured; however, the apparent long-axes of most sand grains are oriented within 45° of the horizontal plane (Fig. S14D).

Cutoff Valley interpretations. – Dark grey bands close to, and parallel to, the sharp lower contact of the till at Site 27 (Fig. 6E) probably record incomplete mixing of sediments as they were transported within the ice as englacial debris (Piotrowski *et al.* 2001), or below the ice as a deforming sediment layer (Boulton *et al.* 2001). This mixing is also evident at the microscale in the form of inter-mixed brown and dark grey plasma (Fig. S14A). This till was probably sourced from a lithologically heterogeneous substrate 'up-ice flow' along Cutoff Valley to the NE of Site 27 and subsequently transported and deposited by glacial ice-forming till. Approximately 3 km NE of Site 27, the bedrock of the Cutoff Valley changes from Palaeozoic and Triassic chert, argillite, siltstone, basalt and andesite to Permian limestone (Roddick *et al.* 1979). This bedrock, and any overlying sediment derived from its weathering and deterioration, may be the source material for the till at Site 27. Turbates and necking structures are indicative of ductile deformation of the till matrix at the microscale, while grain stacks and crushed grains are indicative of increased inter-grain friction and fracturing under low pore-water pressure.

Pavilion plateau and Fraser Plateau macroscale observations. – The till at Site 26 is dark brown, overlies argillite bedrock (Fig. 7C), is heavily fractured with a prismatic structure, and falls apart easily when touched. In one place, the till overlies a till-filled bedrock depression containing striated boulders (Fig. 7C). A shear plane separates the till (containing the boulders) in the bedrock depression from the overlying till from which macrofabrics F28 and F29 were measured (Fig. 7C). Measured striae sets on the upper surfaces of the boulders are oriented ~north–south (Fig. 7C). North-dipping fractures and south-dipping shear planes were measured in the bedrock by Lian & Hicock (2000) (F26a, Fig. 5), but these were covered by debris during examination in this study.

Macrofabric F28 was measured ~30 m north of macrofabric F29. Both macrofabrics have very spread or girdle-like main modes that plunge to the WNW (F28, F29, Fig. 5). A minor secondary mode (M2) shows consistent alignment with the SW dips of some shear planes measured in the underlying bedrock by Lian & Hicock (2000) (F26a, Fig. 5). Fractures in the underlying bedrock dip to the NE (F26a, Fig. 5).

Site 57 is located in a roadcut on the Fraser Plateau that exposes very consolidated till with basalt clasts and steep ~north-, NE- and east-dipping fractures (Figs 5, 6F). The pebble macrofabric shows a very spread ~north–south-trending main mode, and a minor east–west- trending transverse mode (M2) (F19, Fig. 5).

Pavilion plateau and Fraser Plateau micromorphology. – In thin section, the diamicton at Site 26 has many planar voids, is plasma-supported and dominated by subangular to subrounded metasedimentary (argillite) skeletal grains (Table 2; Figs S15, S16). The orientations of major and minor planar voids in thin section S26F29 show no systematic pattern (Table 2; Fig. S16A). Major fractures in thin section S26F28 have a cross-cutting pattern (Table 2; Fig. S15A). Some skeletal grains in both thin sections are aligned subparallel to major planar voids (Figs S15A, S16A). Microfabric domains are straight-to-curvilinear and are randomly oriented (Figs S15C, S16C). Few discrete microstructures were counted at Site 26, but those that were discernible consist of crushed grains, grain lineations and necking structures (Figs S15B, S16B).

In thin section the diamicton at Site 57 appears plasma-supported, and has abundant subrounded to rounded volcanic grains and few subrounded to rounded limestone grains (Fig. S17A). Planar voids are rare but vughs are common (Table 2; Fig. S17A). Crushed grains, turbates, necking structures and grain lineations occur in decreasing order of abundance (Fig. S17B). Most straight and curvilinear microfabric domains have apparent plunges down to the SE (Fig. S17C, D).

Pavilion plateau and Fraser Plateau interpretations. – The fracture and shear planes measured in the bedrock by Lian & Hicock (2000) at Site 26 were interpreted to be associated with glaciotectonic stress and suggest brittle deformation of the substrate as a result of overlying (possibly locally cold-based) north-flowing ice. The ~north–south-trending striae on the upper surfaces of cobbles and boulders (Fig. 7C) suggest that the till within the bedrock depression may have been deposited by north-flowing ice during, or shortly after, the formation of the glaciotectonic features in the bedrock. The spread east–west-trending macrofabric modes from the till that overlies the till-filled depression (F28 and F29, Fig. 5) probably record a local shift in ice-flow direction and/or rotation of pebbles owing to deformation or local compressive stress along the sloping flanks of Pavilion plateau. The shear zone overlying the bedrock depression (Fig. 7C) suggests that basal ice or mobile till probably slid over the bedrock depression after it filled with sediment. The heavily fractured matrix observed in thin sections S26F28 and S26F29 precluded the identification of many discrete microstructures, such as turbates, necking structures and grain lineations (Figs S15A, S15B, S16A, S16B). The subvertical major and minor fractures contribute to the prismatic structure observed at the macroscale. Microfabric domains appear to be influenced by frac-

ture plane orientations (Figs S15A, S15C, S16A, S16C). This structure develops as moist sediment dries out, with subvertical fractures forming when shrinkage forces are largely resolved in a lateral direction (Chadwick & Graham 2000). Freeze–thaw processes have probably led to the shrinking and swelling of the till and to the re-orientation of elongate grains whose long-axes are oriented subparallel to fracture walls (Figs S15A, S16A).

The main mode orientation of the macrofabric measured on the Fraser Plateau (Site 57) is consistent with a SE ice-flow direction as inferred by Plouffe *et al.* (2009, 2011) from streamlined glacigenic landforms (Fig. 1). The steeply dipping fractures measured within the diamicton may be the result of unloading during ice retreat. The roundness of the volcanic skeletal grains (Fig. S17) suggests that they are derived from water-sorted (fluvial) sediments and/or have undergone surface abrasion within the till as it deformed. Discrete microstructure types are dominated by crushed grains (Fig. S17B) that probably underwent fracturing as the till deformed during periods of relatively low pore-water pressure.

Is the microstructure record consistent with previously proposed drainage conditions under the CIS?

Discrete microstructures indicative of microscale ductile deformation (turbates and necking structures) and brittle deformation (grain lineations, grain stacks and crushed grains) are present in most till units examined in this study. In the following section, these data are further analysed quantitatively in order to see if the relative abundances of 'ductile'-type and 'brittle'-type microstructures reflect the proposed till pore-water drainage conditions beneath the CIS. In other words, we test the hypothesis that 'ductile'-type microstructures will dominate in the topographically confined areas and/or in areas on an adverse slope with respect to inferred ice-flow direction (e.g. sites 6, 60, 48 and 27) and that 'brittle'-type microstructures will be relatively more prevalent in topographically unconstrained locations (e.g. sites 26 and 57). We explore whether the complex ice-flow history and the associated possibility of a switch in bed drainage conditions at the north end of Jesmond valley may have affected the microstructures recorded at sites 20 and 23.

Quantitative analysis of microstructures

When comparing the micromorphologies of multiple samples, some studies provide a table with a summary of the observations from individual thin sections, where the presence of each feature is recorded and the abundance or degree of development is indicated (e.g. Carr 2001; Hart *et al.* 2004; Baroni & Fasano 2006; Hart

2006a). Some studies count the total number of microstructures present within a representative area of each thin section (Larsen *et al.* 2006a, b, 2007; Menzies *et al.* 2006; Menzies & Whiteman 2009; Reinardy *et al.* 2011). When the absolute number of microstructures is counted, the relative frequencies of different microstructure types are typically tabulated or shown in histograms or line charts (e.g. Larsen *et al.* 2006a, b, 2007; Menzies & Whiteman 2009). More in-depth statistical analyses of the data are rarely attempted. In 2006, a statistical method of analysing counted microstructures was introduced for the purpose of differentiating between diamicton types (Menzies *et al.* 2006; Menzies & Whiteman 2009). This involved comparing microstructure data from a range of different diamictons using the Chi-square test. The Chi-square test tests one diamicton against another using a null hypothesis that no statistical difference exists between any two of the sample data sets, implying that both diamictons come from the same population and therefore formed under similar conditions. In order to obtain statistically significant results, Menzies *et al.* (2006) counted microstructures from a large number (26–81) of thin sections from each diamicton. The level of subjectivity involved in microstructure identification was not assessed, and microstructures were counted from only a 400 mm² area in each thin section.

Because observations in this study were restricted to a low number (1–4) of thin sections from each sample site, and because all till units sampled are thought to be part of a single subglacial till unit (Kamloops Lake till), sample sites were not tested against each other using Chi-square statistical analysis. Rather, an exploratory data analysis approach was undertaken using multivariate hierarchical cluster analysis (Everitt 1993). The advantage of this approach is that it enables the detection of levels of similarity or difference between thin sections that may be indicative of spatial and/or temporal variations in subglacial conditions recorded in a single till unit (in this case, Kamloops Lake till). When applied to a suite of thin sections sampled from a single till unit over a wide geographic area, such as in this study, this technique can expose relationships that may exist between till micromorphology and the geomorphology of the study area. A limitation of this approach is that it is dependent on the relative abundance of certain microstructures, which, in turn, is somewhat dependent on till granulometry and void spacing. If, as discussed below, the number of voids is large in a thin section, then this will obviously limit the number of microstructures that can be counted.

For the purposes of cluster analysis, the absolute numbers of turbates, necking structures, grain lineations, grain stacks and crushed grains were counted in all thin sections examined (Table 3). To maximize counting statistics, microstructures were counted from the entire area of each thin section rather than from a

Table 3. Microstructure associations (MAs) for all thin sections examined in this study.

MA[1]	Thin section sampling area (cm^2)	N[2]	Turbates (%)	Necking structures (%)	Grain lineations (%)	Grain stacks (%)	Crushed grains (%)	Cluster group
Northern Jesmond valley								
S23F30	24	20	45	15	20	20	0	3
S23F31	23	16	56	13	25	6	0	2
S20F7	25	34	85	6	0	3	6	3
Edge Hills								
S6F26	27	42	31	38	24	2	5	4
S6F27	25	57	35	37	11	11	7	3
S6F33	25	15	40	20	27	0	13	1
Southern Jesmond valley								
S60F11	26	73	68	1	11	16	3	2
S60F13	27	79	75	3	5	11	6	6
S60F14	24	31	29	29	26	6	10	7
S60F15	23	49	27	43	20	2	8	2
S48F9	20	34	53	12	15	9	12	3
S48F10	25	67	63	12	12	6	7	3
S48F17	28	46	30	26	4	28	11	3
S48F32	26	57	60	19	9	12	0	3
Cutoff Valley								
S27F1	24	65	23	46	18	0	12	3
Pavilion and Fraser plateaus								
S26F28	29	3	0	33	33	0	33	5
S26F29	27	8	0	0	38	0	63	5
S57F19	24	25	16	12	12	0	60	4

[1]Each MA is labelled after the site location (S#) and macrofabric sampling area (F#) from which the thin sectioned till was derived.
[2]N refers to the total number of microstructures counted.

smaller representative area. The average sampling area was 25 ± 2 cm^2 (Table 3). Using these data, the relative proportion of each microstructure type (out of 100%) was calculated for each thin section. For example, if 46 microstructures were counted from a thin section, and 14 of these were turbates, then the relative proportion of turbates for that thin section is (14/46)×100%=30%. The array of values that constitutes the percentages of all five microstructure types for each thin section is referred to here as a microstructure association (MA). All MAs for all 18 thin sections are listed in Table 3. Because each MA is an array of percentage values with a sum of 100%, all MAs were clustered using techniques designed for compositional data (Aitchison 1986). This statistical protocol is outlined in Appendix A.

Cluster analysis results. – The similarity between all MAs is illustrated in the dendrogram in Fig. 9.
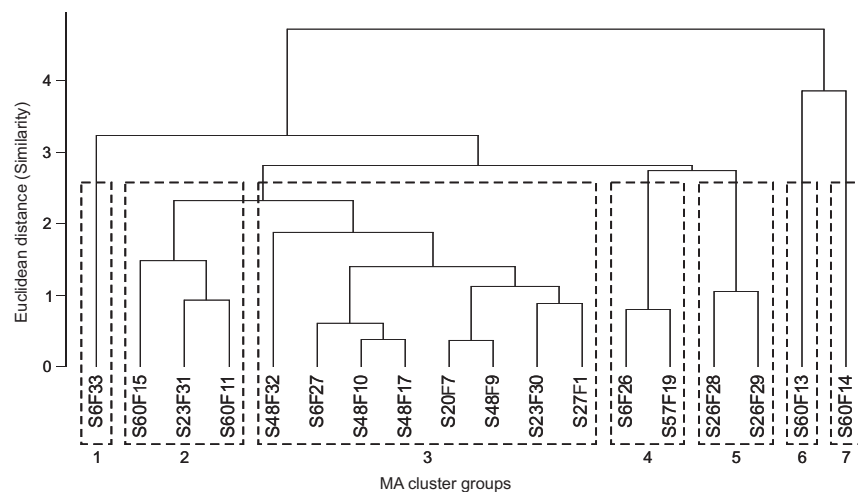

Fig. 9. Dendrogram showing hierarchical cluster analysis of all microstructure associations (MAs). Each MA is labelled after the site location (S#) and macrofabric sampling area (F#) from which the thin-sectioned till was derived. The resulting MA clusters have been divided into seven groups (dashed boxes).
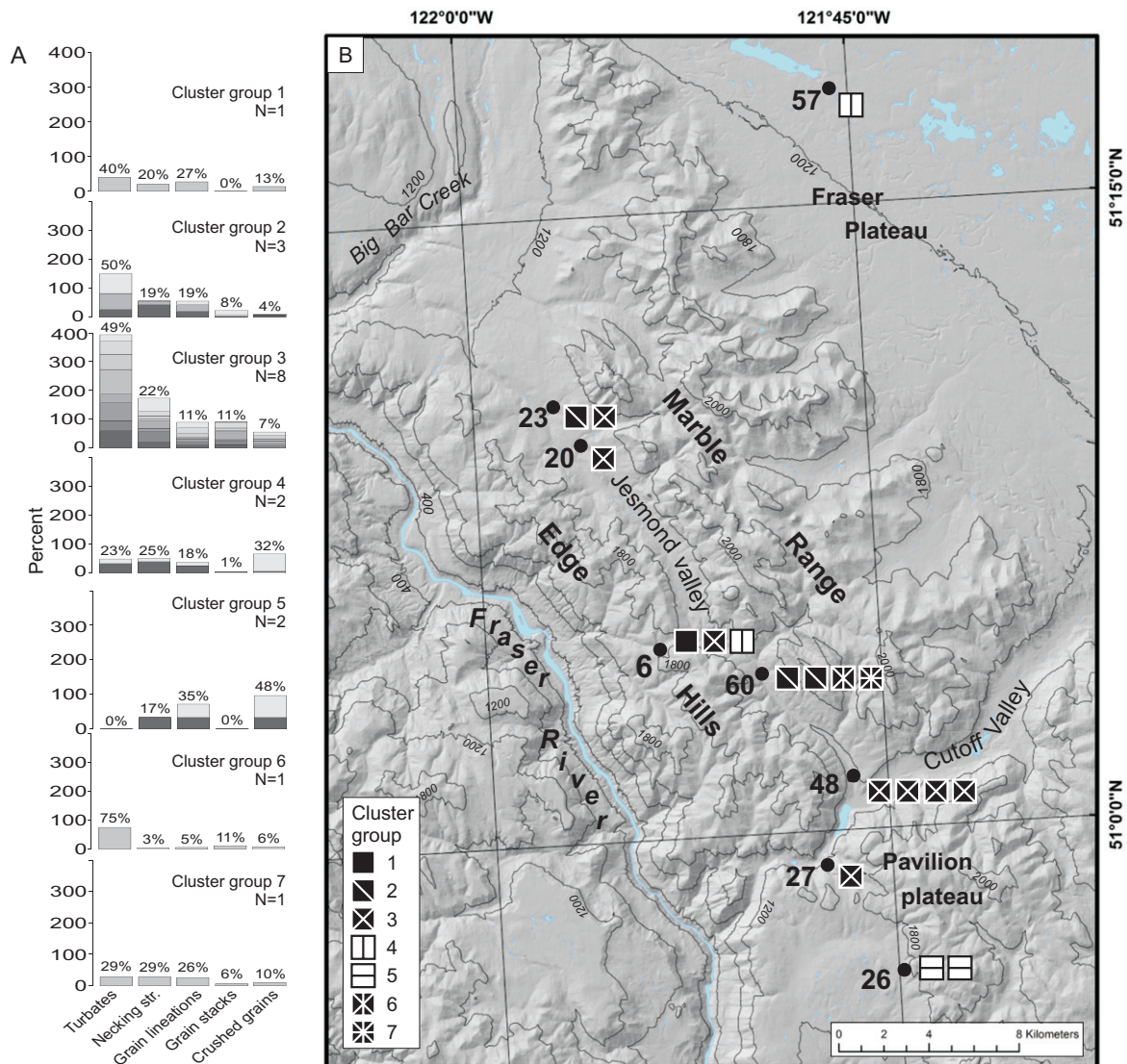
Fig. 10. A. Stacked bar plots for each of the seven microstructure association (MA) cluster groups in Fig. 9. Each MA, consisting of the relative proportions of all five microstructure types (in percent), is given a different grey tone and all MAs in each group are stacked one on top of the other. N is the total number of MAs in each group, and the array of values above each stack is the average relative proportion of microstructures in each group. B. The geography of MA cluster groups for all sites examined. Cluster groups comprising at least 50% 'ductile'-type microstructures are shown as black-filled symbols with white lines. All others are shown as white-filled symbols with black lines. See Fig. 9 for the cluster dendrogram. This figure is available in colour at http://www.boreas.dk.

Dendrograms are tree diagrams that illustrate the arrangement of clusters produced by hierarchical clustering. MA clusters were divided into seven groups (cluster groups 1–7, Fig. 9), and the microstructure composition as well as the geographic distribution of each are shown in Fig. 10. Ductile-type microstructures, typically dominated by turbates, are best represented in cluster groups 1, 2, 3, 6 and 7, where they constitute at least 50% of all microstructures counted (Fig. 10A).

In topographically constrained areas or in areas with an adverse slope at the LGM (sites 60, 48, 27 and 6) all

thin sections are dominated by ductile structures, as expected (black symbols, Fig. 10B). Thin section S6F26 falls into group 4 (white symbol, Fig. 10B), but 69% of its microstructures are ductile. The cluster analysis probably groups thin sections S6F26 and S57F19 together because the relative proportions of turbates and necking structures are similar (i.e. only 7% difference between turbates and necking structures in S6F26, and 4% difference between turbates and necking structures in thin section S57F19) and both have grain stacks that constitute 1% or less of all counted microstructures. Intra-till variation in the

relative proportions of microstructures is observed at sites 60 and 6 (Table 3; Figs 6C, 7, 10). Thin sections in the lower two-thirds of the till layer exposed at Site 60, exposure 2 fall into cluster groups 2 and 6 and have a relatively high amount of ductile-type microstructures that are dominated by turbates (Table 3; Figs 7A, 10). The thin section closest to the upper contact of this till falls into group 7, which has turbates, necking structures and grain lineations in roughly equal proportions (29 and 26%) followed by fewer grain stacks (6%) and crushed grains (10%) (Figs 7A, 10), suggesting a slightly less ductile (more brittle) microstructure record. The three thin sections at Site 6 fall into three different cluster groups (groups 1, 3 and 4). Thin sections near macrofabrics F26 and F27 (close to the fold, Fig. 6C) are both dominated by turbates and necking structures, with ductile-type microstructures representing 69 and 72%, respectively, of all microstructures counted. The thin section near macrofabric F33 (~20 m east of F27) is dominated by turbates and grain lineations, with ductile-type microstructures representing 60% of all microstructures counted. At Site 48, all thin sections fall into cluster group 3 (Table 3; Figs 7B, 10).

Thin sections from topographically unconstrained areas on the plateaus (sites 26 and 57) are dominated by crushed grains and grain lineations (groups 4 and 5, Table 3; Fig. 10), suggesting a much more brittle microscale deformation history, as we might expect. However, it is noted that, owing to the low number of microstructures counted, particularly at Site 26, the calculated MAs should be interpreted with caution. Both MAs from Site 26 fall into cluster group 5 and have fewer than 10 countable microstructures (Table 3; Fig. 10). The low frequency of microstructures within these MAs may be attributed to a high frequency of voids in the till matrix. The fact that the cluster analysis technique singles out thin sections with low microstructure counts is not a flaw in the statistical technique itself, because these thin sections do have distinct MAs. However, it does show that if cluster analysis is to be used to extract variations in subglacial conditions/processes, then ideally we should restrict our observations to samples with similar granulometry, and a minimum number of voids that will limit microstructure counts.

The till matrix in the northern part of Jesmond valley is dominated by ductile-type microstructures (mostly turbates, groups 2 and 3). Site 23 has a moderate (20–25%) proportion of grain lineations, while Site 20 has none (Table 3). Crushed grains are absent at Site 23, but a few (~6%) were identified at Site 20 (Table 3; Fig. 10). The prominent ductile signature at these sites may be attributed to earlier poorly drained conditions associated with ice advance against an adverse slope to the SE, as inferred from observations at Site 20 by Lian & Hicock (2000).

To summarise, cluster analysis seems to support previously proposed drainage conditions: till thin sections from topographically constrained areas and/or areas with adverse slopes with respect to the ice-flow direction are typically dominated by ductile-type microstructures, as expected in areas of poor bed drainage, whereas thin sections from the topographically unconstrained plateaus are dominated by brittle-type microstructures, as expected under better-drained subglacial conditions (Fig. 10). As discussed below, examination of the till micromorphology on the plateaus suggests that the frequency and distribution of voids in the till matrix, till texture and skeletal grain shapes may adversely affect the preservation potential of microstructures.

Till formation and subglacial conditions under the CIS in the study area

Macroscale evidence

Macroscale observations of Kamloops Lake till in the study area show that till accumulation beneath the CIS in this region probably occurred through a combination of lodgement and deformation processes in a temperate subglacial environment characterised by fluctuating pore-water pressures. The presence of long-axis-parallel striae on the upper surfaces of individual clasts, and clast facets and stoss and lee ends suggest that clasts at all sites experienced phases of ploughing, lodgement, plucking and abrasion under sliding CIS ice (cf. Krüger 1984). Plucking and abrasion of clasts probably occurred within shear zones at, or close to, the ice-bed interface (Tulaczyk 1999; Piotrowski *et al.* 2006). Most main macrofabric modes, particularly those associated with a principal eigenvalue of 0.70 or higher, probably record the preferential alignment of pebble a-axes to the local shear direction of the substrate (Iverson *et al.* 2008). Many modes are oriented parallel or subparallel to the local valley axes, and thus probably record local ice-flow patterns as suggested by Lian & Hicock (2000) (Fig. 1). The spread nature of the macrofabric modes, and the inconsistent stoss and lee end directions of stones in till studied at most sites in the study area may be attributed to local shifts in ice-flow direction (cf. MacClintock & Dreimanis 1964; Hicock & Lian 1999; Lian & Hicock 2000, 2010), to re-orientation of till clasts as a result of their collision with lodged clasts at the ice-bed interface, or to re-orientation as a result of subsequent ductile deformation of a dilated till horizon during periods of high pore-water pressure (Hicock *et al.* 1996; Hart 2006b).

The strongest evidence for ductile deformation is present in the Edge Hills (Site 6) and in the southern part of Jesmond valley (Site 60), supporting Lian & Hicock's (2000) conclusion that till deposited in topographically confined areas and on adverse slopes at glacial maximum (Fig. 1) was more prone to elevated

subglacial pore-water pressures. However, even these sites contain macroscale evidence that indicates that brittle deformation followed the interval of ductile deformation. At Site 6, evidence for ductile deformation appears in the form of a fold in the till matrix (Fig. 6C). At Site 60, evidence for ductile deformation appears in the form of well-preserved entrained, and in places imbricated, pebbly siltstone and sandstone bedrock clasts (Fig. 8) and very spread or girdle-like macrofabric modes. Evidence for brittle deformation at sites 6 and 60 consists of macroscale shear and fracture planes (Figs 6D, 7A), clast facets and upper-surface striae parallel to clast a-axes and the preferential orientation of pebbles with the local valley wall or axis (the presumed orientation of ice flow) (Figs 1, 5). Ductile deformation of dilated till in the Edge Hills and the southern part of Jesmond valley appears therefore to have been followed by drainage of the substrate beneath the CIS and a return to brittle deformation processes (evidenced by the fracture and shear planes at Site 60 and the shear plane at Site 6).

At Site 48, near the southern end of Jesmond valley, spread and girdle-like macrofabrics similar to those at Site 60 are present in the till, but other evidence for ductile deformation is lacking despite this site's location on an adverse slope relative to the inferred ice-flow direction (Fig. 1). This could be because the till could not be viewed in close proximity to its lower contact with underlying sediments and/or bedrock (which was not exposed), where evidence of ductile deformation would be expected to be most visible.

At Site 27, where till would have accumulated in a relatively topographically constricted area in Cutoff Valley, possible evidence for ductile deformation includes the dark grey subhorizontal bands that appear near the lower contact (Fig. 6E). These could be interpreted as attenuation features that formed in a ductilely deforming sediment layer (e.g. cf. Boulton *et al.* 2001: fig. 2). An alternative interpretation of these bands is that they were produced during deformation of debris-rich ice and were preserved during melt-out of the ice forming till (Lawson 1979; Shaw 1979), but clear evidence for the melt-out of interstitial ice in the form of water escape structures and/or sorted sediments is lacking in thin section S27F1 (Fig. S14).

Macroscale evidence of brittle deformation under well-drained conditions under the CIS in the study area is present in shear and/or fracture planes in most tills, and in the subtill substrate if it is visible (e.g. sites 20, 6, 60, 48, 26 and 57). At sites 60 and 26, glaciotectonic features in the subtill bedrock are evidence of shearing and fracturing of the substrate under well-drained, possibly cold-based conditions during the arrival of the glacial margin and before the accumulation of till. Long (>1 m) shear and fracture planes penetrating the uppermost few metres of till at sites 48 and 60 (Fig. 7A, B) are consistent with the dewatering and brittle failure

of these units after much or most of the till had been deposited. In the wider, northern end of Jesmond valley, where the slope declines in the direction of the inferred LGM ice-flow direction, subhorizontal fissility planes and silt-filled fracture and shear planes observed in till at the macroscale record brittle deformation under well-drained conditions (sites 20 and 23, Figs 1, 6A, B). Macroscale evidence of ductile deformation was not observed at sites examined in the northern part of Jesmond valley.

Microscale evidence

At the microscale, Kamloops Lake till experienced both brittle and ductile deformation. Turbates and necking structures are indicative of grain rotation and squeeze flow of sediment between grains under moist conditions, and microshears, grain stacks and crushed grains suggest that microshearing, grain stacking and grain fracturing occurred under well-drained conditions (Menzies 2000; Larsen *et al.* 2006a). The presence of both types of microstructures in most thin sections is consistent with microscale observations of subglacial tills reported in the literature (e.g. Piotrowski *et al.* 2006; Hart 2006a; Menzies & Brand 2007) and may be indicative of temporal and/or spatial changes in pore-water pressure within the till matrix. Ductile deformation, leading to the rotation of stiff elements and squeeze flow of the till matrix, probably occurred during episodes of elevated pore-water pressure within distributed zones of deformation (Iverson *et al.* 1998; Iverson & Iverson 2001; Menzies 2012). As pore-water pressures dropped, increased friction between grains probably led to microshearing and grain stacking (Hooke & Iverson 1995; Thomason & Iverson 2006). High stresses between adjacent grains would have developed in well-drained conditions, leading to grain crushing (Hooke & Iverson 1995; Hiemstra & van der Meer 1997; Piotrowski *et al.* 2006).

Sites 6 and 60 in the Edge Hills and the southern part of Jesmond valley have the strongest macroscale evidence for ductile deformation and may therefore be expected to exhibit significant evidence of ductile deformation at the microscale. This is certainly the case (Table 3; Fig. 10). However, ductile-type microstructures represent a significant proportion of nearly all thin sections examined from topographically constrained sites. This prevalence of ductile-type microstructures in nearly all till samples examined suggests either that the microscale ductile deformation signature was preserved after subsequent macroscale brittle deformation (as evidenced by the large shear and fracture planes, Fig. 7A, B) and/or that lodgement processes result in both brittle and ductile microstructures (Piotrowski *et al.* 2006; Menzies 2012) (e.g. sites 20 and 23).

Thin sections from till sampled on Pavilion plateau and the Fraser Plateau are dominated by grain linea-

tions and crushed grains (Table 3; Fig. 10). However, micromorphological examination of these tills suggests that the preservation potential of microstructures at these sites may be adversely affected either by a large number of voids in the till matrix or by skeletal grain shapes. On the Pavilion plateau, very few (<10) microstructures were identified in thin section. Microscopic examination of the till matrix at Site 26 suggests that fracturing of the matrix owing to freeze–thaw action and/or unloading (Figs S5A, S15A, S16A) may have limited the preservation potential of microstructures, leading to low counting statistics and consequent MAs that would not be representative of the till had it not experienced fracturing. At Site 57 (Fraser Plateau), sand to granule-sized volcanic grains observed in the thin section are typically subrounded and equidimensional (Fig. S17A). Because there are few elongate grains that may become aligned to the edges of larger grains, turbates and necking structures are rare (Fig. S17B).

The co-existence, and often the superimposition, of brittle and ductile deformation signatures observed at the macro- and microscales in till associated with the CIS is consistent with current models of till accumulation under warm-based (temperate) glaciers (Piotrowski *et al.* 2004, 2006; Larsen *et al.* 2007; Menzies 2012). Proponents of these models argue that till formation under temperate glaciers is likely to occur in environments where frequent switches between sliding at the ice-bed interface and deformation of the substrate (owing to ice-bed coupling) can occur in response to changes in pore-water pressure in the till or in water pressure at the ice-bed interface (Iverson *et al.* 1999; Truffer & Harrison 2006; Stokes *et al.* 2007). The superimposition of brittle and ductile deformation structures can also occur through vertical migration of the subglacial deforming layer during till accretion (Larsen *et al.* 2004), through the migration of shear zones within the deforming till layer (Iverson *et al.* 1998), through dewatering of the sediment (Phillips *et al.* 2007), or through dilatant strengthening (Moore & Iverson 2002). Modes of till deformation may switch from brittle to ductile, and back again, and both modes of deformation can occur in tills simultaneously, but at different scales (Menzies 2000, 2012; Passchier & Trouw 2006). Unfortunately, the data collected in this study do not allow us to constrain the maximum depth of deformation at any one time.

Conclusions

This paper presents the first integrated macroscale and microscale examination of subglacial till associated with the CIS. A new statistical approach to quantifying till micromorphology (multivariate hierarchical cluster analysis for compositional data) is also described and implemented. The advantage of this approach is that it enables the detection of levels of similarity or difference between thin sections that may be indicative of spatial and/or temporal variations in subglacial conditions recorded in a single till unit (in this case, Kamloops Lake till). When applied to a suite of thin sections sampled from a single till unit over a wide geographic area, this technique can expose relationships that may exist between till micromorphology and the geomorphology of the study area.

Sedimentological observations made at the macro- and microscale support previous assertions based on more-limited data that the till in this region formed through a combination of lodgement and deformation processes in a temperate subglacial environment. The data presented here show that subglacial environments below the CIS were influenced by topography, whereby poor drainage of the substrate in topographically constricted areas or on adverse slopes facilitated ductile deformation of the glacier bed (Lian & Hicock 2000; Lian *et al.* 2003). Cluster analysis of microstructure data together with qualitative observations made from thin sections suggest that the relative frequency of microstructures in this till unit was probably influenced by topography in relation to ice-flow direction (bed drainage condition) as well as by the frequency and distribution of voids in the till matrix and skeletal grain shapes. This study reinforces the notion that the detailed examination of micro- and macro-features can lead to a greater understanding of the processes that occurred beneath glaciers and ice sheets, particularly in topographically complex regions such as that of the CIS.

References

Aitchison, J. 1986: *The Statistical Analysis of Compositional Data.* 416 pp. Chapman and Hall, London.

Alley, R. B. & Bindschadler, R. A. 2001: The West Antarctic Ice Sheet and sea level change. *In* Alley, R. B. & Bindschadler, R. A. (eds): *The West Antarctic Ice Sheet: Behavior and Environment*, 1–11. *American Geophysical Union, Antarctic Research Series 77*, Washington, DC.

Baroni, C. & Fasano, F. 2006: Micromorphological evidence of warm-based glacier deposition from the Ricker Hills Tillite (Victoria Land, Antarctica). *Quaternary Science Reviews 25*, 976–992.

Benn, D. I. 1995: Fabric signature of subglacial till deformation, Breidamerkurjökull, Iceland. *Sedimentology 42*, 735–747.

Benn, D. I. & Evans, D. J. A. 1998: *Glaciers and Glaciation*. 734 pp. Arnold, London.

Bertler, N. A. N. & Barrett, P. J. 2010: Vanishing ice sheets. *In* Dodson, J. (ed.): *Changing Climates, Earth Systems, and Society*, 49–83. Springer: Warren, Michigan, United States of America.

van den Boogaart, K. G. & Tolosana-Delgado, R. 2008: 'compositions': A unified R package to analyze compositional data. *Computers & Geosciences 34*, 320–338.

Boulton, G. S. 1975: Processes and patterns of subglacial sedimentation: a theoretical approach. *In* Wright, A. E. & Moseley, F. (eds): *Ice Ages: Ancient and Modern*, 7–42. Seel House Press, Liverpool.

Boulton, G. S. & Hindmarsh, R. C. A. 1987: Sediment deformation beneath glaciers: rheology and geological consequences. *Journal of Geophysical Research 92*, 9059–9082.

Boulton, G. S. & Jones, A. S. 1979: Stability of temperate ice caps and ice sheets resting on deformable sediment. *Journal of Glaciology 24*, 29–43.

Boulton, G. S., Dobbie, K. E. & Zatsepin, S. 2001: Sediment deformation beneath glaciers and its coupling to the subglacial hydraulic system. *Quaternary International 86*, 3–28.

Brewer, R. 1976: *Fabric and Mineral Analysis of Soils*. 482 pp. Kreiger, Huntington, NY.

Broster, B. E. 1991: Glacitectonic deformation in sediment and bedrock, Hat Creek, British Columbia. *Géographie physique et Quaternaire 45*, 5–20.

Broster, B. E. & Clague, J. J. 1987: Advance and retreat glacigenic deformation at Williams Lake, British Columbia. *Canadian Journal of Earth Sciences 24*, 1421–1430.

Broster, B. E., Dreimanis, A. & White, J. C. 1979: A sequence of glacial deformation, erosion, and deposition at the ice-rock interface during the last glaciation: Cranbrook, British Columbia, Canada. *Journal of Glaciology 23*, 645–657.

Brown, N. E., Hallet, B. & Booth, D. B. 1987: Rapid soft bed sliding of the Puget glacial lobe. *Journal of Geophysical Research 92*, 8985–8997.

Carr, S. 2001: Micromorphological criteria for discriminating subglacial and glacimarine sediments: evidence from a contemporary tidewater glacier, Spitsbergen. *Quaternary International 86*, 71–79.

Carr, S. J. & Lee, J. A. 1998: Thin-section production of diamicts; problems and solutions. *Journal of Sedimentary Research, Section A: Sedimentary Petrology and Processes 68*, 217–220.

Chadwick, O. A. & Graham, R. C. 2000: Pedogenic processes. *In* Sumner, M. E. (ed.): *Handbook of Soil Science*, E.41–E.75. CRC Press, Boca Raton, FL.

Clague, J. J. & James, T. S. 2002: History and isostatic effects of the last ice sheet in southern British Columbia. *Quaternary Science Reviews 21*, 71–87.

Clague, J. J., Ryder, J. M., Matthews, W. H., Hughes, O. L., Rutter, N. W., Jackson, L. E., Matthews, J. V., Jr & MacDonald, G. M. 1989: Quaternary geology of the Canadian Cordillera. *In* Fulton, R. J. & Wheeler, J. O. (eds): *Quaternary Geology of Canada and Greenland*, 15–96. Geological Survey of Canada, Ottawa.

Dreimanis, A. 1989: Tills; their genetic terminology and classification. *In* Goldthwait, R. & Matsch, C. L. (eds): *Genetic Classification of Glacigenic Deposits*, 17–96. A. A. Balkema, Rotterdam.

Elson, J. A. 1989: Comment on glacitectonite, deformation till, and comminution till. *In* Goldthwait, R. & Matsch, C. L. (eds): *Genetic Classification of Glacigenic Deposits*, 85–88. A. A. Balkema, Rotterdam.

Evans, D. J. A., Phillips, E. R., Hiemstra, J. F. & Auton, C. A. 2006: Subglacial till: formation, sedimentary characteristics and classification. *Earth Science Reviews 78*, 115–176.

Everitt, B. 1993: *Cluster Analysis*. 170 pp. Halsted Press, London.

Fulton, R. J. & Smith, G. W. 1978: Late Pleistocene stratigraphy of south-central British Columbia. *Canadian Journal of Earth Sciences 15*, 971–980.

Hart, J. & Rose, J. 2001: Approaches to the study of glacier bed deformation. *Quaternary International 86*, 45–58.

Hart, J. K. 1994: Till fabric associated with deformable beds. *Earth Surface Processes and Landforms 19*, 15–32.

Hart, J. K. 2006a: An investigation of subglacial processes at the microscale from Briksdalsbreen, Norway. *Sedimentology 53*, 125–146.

Hart, J. K. 2006b: Athabasca Glacier, Canada; a field example of subglacial ice and till erosion? *Earth Surface Processes and Landforms 31*, 65–80.

Hart, J. K. & Boulton, G. S. 1991: The interrelationship between glaciotectonic deformation and glaciodeposition. *Quaternary Science Reviews 10*, 335–350.

Hart, J. K., Khatwa, A. & Sammonds, P. 2004: The effect of grain texture on the occurrence of microstructural properties in subglacial till. *Quaternary Science Reviews 23*, 2501–2512.

Hicock, S. R. & Dreimanis, A. 1985: Glaciotectonic structures as useful ice-movement indicators in glacial deposits: four Canadian case studies. *Canadian Journal of Earth Sciences 22*, 339–346.

Hicock, S. R. & Dreimanis, A. 1992: Deformation till in the Great Lakes region; implications for rapid flow along the south-central margin of the Laurentide Ice Sheet. *Canadian Journal of Earth Sciences 29*, 1565–1579.

Hicock, S. R. & Fuller, E. A. 1995: Lobal interactions, rheologic superposition, and implications for a Pleistocene ice stream on the continental shelf of British Columbia. *Geomorphology 14*, 167–184.

Hicock, S. R. & Lian, O. B. 1999: Cordilleran Ice Sheet lobal interactions and glaciotectonic superposition through stadial maxima along a mountain front in southwestern British Columbia, Canada. *Boreas 28*, 531–542.

Hicock, S. R., Goff, J. R., Lian, O. B. & Little, E. C. 1996: On the interpretation of subglacial till fabric. *Journal of Sedimentary Research 66*, 928–934.

Hiemstra, J. F. & van der Meer, J. J. M. 1997: Pore-water controlled grain fracturing as an indicator for subglacial shearing in tills. *Journal of Glaciology 43*, 446–454.

Hiemstra, J. F. & Rijsdijk, K. F. 2003: Observing artificially induced strain; implications for subglacial deformation. *Journal of Quaternary Science 18*, 373–383.

Hooke, R. L. & Iverson, N. R. 1995: Grain-size distribution in deforming subglacial tills; role of grain fracture. *Geology 23*, 57–60.

Huntley, D. H. & Broster, B. E. 1993: Polyphase glacigenic deformation of advance glaciofluvial sediments near Big Creek, British Columbia. *Géographie physique et Quaternaire 47*, 211–219.

Iverson, N. R. & Iverson, R. M. 2001: Distributed shear of subglacial till due to Coulomb slip. *Journal of Glaciology 47*, 481–488.

Iverson, N. R., Baker, R. W., Hooke, R. L., Hanson, B. & Jansson, P. 1999: Coupling between a glacier and a soft bed; I, A relation between effective pressure and local shear stress determined from till elasticity. *Journal of Glaciology 45*, 31–40.

Iverson, N. R., Hooyer, T. S. & Baker, R. W. 1998: Ring-shear studies of till deformation; Coulomb-plastic behavior and distributed strain in glacier beds. *Journal of Glaciology 44*, 634–642.

Iverson, N. R., Hooyer, T. S., Thomason, J. F., Graesch, M. & Shumway, J. R. 2008: The experimental basis for interpreting particle and magnetic fabrics of sheared till. *Earth Surface Processes and Landforms 33*, 627–645.

Khatwa, A. & Tulaczyk, S. 2001: Microstructural interpretations of modern and Pleistocene subglacially deformed sediments; the relative role of parent material and subglacial processes. *Journal of Quaternary Science 16*, 507–517.

Kilfeather, A. A. & van der Meer, J. J. M. 2008: Pore size, shape and connectivity in tills and their relationship to deformation processes. *Quaternary Science Reviews 27*, 250–266.

Kilfeather, A. A., O'Cofaigh, C., Dowdeswell, J. A., van der Meer, J. J. M. & Evans, D. J. A. 2010: Micromorphological characteristics of glacimarine sediments: implications for distinguishing genetic processes of massive diamicts. *Geo-Marine Letters 30*, 77–97.

Krüger, J. 1984: Clasts with stoss-lee form in lodgement tills: a discussion. *Journal of Glaciology 30*, 241–243.

Larsen, N. K., Piotrowski, J. A. & Christiansen, F. 2006b: Microstructures and microshears as proxy for strain in subglacial

diamicts: implications for basal till formation. *Geology 34*, 889–892.

Larsen, N. K., Piotrowski, J. A., Christoffersen, P. & Menzies, J. 2006a: Formation and deformation of basal till during a glacier surge; Elisabreen Svalbard. *Geomorphology 81*, 217–234.

Larsen, N. K., Piotrowski, J. A. & Kronborg, C. 2004: A multiproxy study of a basal till: a time-transgressive accretion and deformation hypothesis. *Journal of Quaternary Science 19*, 9–21.

Larsen, N. K., Piotrowski, J. A. & Menzies, J. 2007: Microstructural evidence of low-strain, time-transgressive subglacial deformation. *Journal of Quaternary Science 22*, 593–608.

Lawson, D. E. 1979: A comparison of the pebble orientations in ice and deposits of the Matanuska Glacier, Alaska. *Journal of Geology 87*, 629–645.

Lee, J. A. & Kemp, R. A. 1992: Thin sections of unconsolidated sediments and soils: a recipe. *CEAM Technical Report 2*, 32 pp. University of London, Royal Holloway.

Lian, O. B. 1997: *Quaternary geology of the Fraser Valley area, south-central B.C.* Ph.D. thesis, University of Western Ontario, 489 pp.

Lian, O. B. & Hicock, S. R. 2000: Thermal conditions beneath parts of the last Cordilleran Ice Sheet near its centre as inferred from subglacial till, associated sediments, and bedrock. *Quaternary International 68–71*, 147–162.

Lian, O. B. & Hicock, S. R. 2001: Lithostratigraphy and limiting optical ages of the Pleistocene fill in Fraser River valley near Clinton, south-central British Columbia. *Canadian Journal of Earth Sciences 38*, 839–850.

Lian, O. B. & Hicock, S. R. 2010: Insight into the character of palaeo-ice-flow in upland regions of mountain valleys during the last major advance (Vashon Stade) of the Cordilleran Ice Sheet, southwest British Columbia, Canada. *Boreas 39*, 171–186.

Lian, O. B., Hicock, S. R. & Dreimanis, A. 2003: Laurentide and Cordilleran fast ice flow: some sedimentological evidence from Wisconsinan subglacial till and its substrate. *Boreas 32*, 102–113.

Linch, L. D. & van der Meer, J. J. M. 2012: Metripol birefringence imaging of unconsolidated glaciotectonized and ice keel scoured sediments: identification of unistrial plasmic fabric. *Boreas*, DOI: 10.1111/j.1502-3885.2012.00290.x.

MacClintock, P. & Dreimanis, A. 1964: Orientation of till fabric by overriding glacier in the Saint Lawrence Valley. *American Journal of Science 262*, 133–142.

Martín-Fernández, J. A., Barceló-Vidal, C. & Pawlowsky-Glahn, V. 1998a: A critical approach to non-parametric classification of compositional data. *In* Rizzi, A., Vichi, M. & Bock, H.-H. (eds): *Advances in Data Science and Classification. Proceedings of the 6th Conference of the International Federation of Classification Societies*, 49–56. Springer-Verlag, Berlin.

Martín-Fernández, J. A., Barceló-Vidal, C. & Pawlowsky-Glahn, V. 1998b: Measures of difference for compositional data and hierarchical clustering methods. *In* Buccianti, A., Nardi, G. & Potenza, R. (eds): *The Fourth Annual Conference of the International Association for Mathematical Geology*, 526–531. De Frede Editore, Napoli.

Martín-Fernández, J. A., Barceló-Vidal, C. & Pawlowsky-Glahn, V. 2003: Dealing with zeros and missing values in compositional data sets using nonparametric imputation. *Mathematical Geology 35*, 253–278.

van der Meer, J. J. M. 1987: Micromorphology of glacial sediments as a tool in distinguishing genetic varieties of till. *Geological Survey of Finland, Special Paper 3*, 77–89.

van der Meer, J. J. M. 1993: Microscopic evidence of subglacial deformation. *Quaternary Science Reviews 12*, 553–587.

van der Meer, J. J. M. 1996: Micromorphology. *In* Menzies, J. (ed.): *Past Glacial Environments, Sediments, Forms, and Techniques, Glacial Environments II*, 335–355. Butterworth-Heineman, Oxford.

van der Meer, J. J. M. 1997: Particle and aggregate mobility in till: Microscopic evidence of subglacial processes. *Quaternary Science Reviews 16*, 827–831.

van der Meer, J. J. M. & Menzies, J. 2006: *Handbook Sixth International Workshop on the Micromorphology of Glacial Sediments.*

83 pp. Department of Geosciences, Hamilton College, Clinton, NY.

van der Meer, J. J. M. & Menzies, J. 2011: The micromorphology of unconsolidated sediments. *Sedimentary Geology 238*, 213–232.

van der Meer, J. J. M., Menzies, J. & Rose, J. 2003: Subglacial till; the deforming glacier bed. *Quaternary Science Reviews 22*, 1659–1685.

Menzies, J. 2000: Micromorphological analyses of microfabrics and microstructures indicative of deformation processes in glacial sediments. *In* Maltman, A. J., Hubbard, B. & Hambrey, M. J. (eds): *Deformation of glacial materials*, 245–257. Geological Society, London, Special Publication 176.

Menzies, J. 2012: Strain pathways, till internal architecture and microstructures – perspectives on a general kinematic model – a 'blueprint' for till development. *Quaternary Science Reviews 50*, 105–124.

Menzies, J. & Brand, U. 2007: The internal sediment architecture of a drumlin, Port Byron, New York State, USA. *Quaternary Science Reviews 26*, 322–335.

Menzies, J. & Maltman, A. J. 1992: Microstructures in diamictons—evidence of subglacial bed conditions. *Geomorphology 6*, 27–40.

Menzies, J. & Whiteman, C. 2009: A comparative analyses of microstructures from Late Jurassic diamictic units, near Helmsdale, northeast Scotland and a Pleistocene diamicton from near Milton, southern Ontario, Canada – a differential diagnostic method of sediment *typing* using micromorphology. *Netherlands Journal of Geosciences 88*, 75–94.

Menzies, J., van der Meer, J. J. M. & Rose, J. 2006: Till – as a glacial 'tectomict', its internal architecture, and the development of a 'typing' method for till differentiation. *Geomorphology 75*, 172–200.

Moore, P. L. & Iverson, N. R. 2002: Slow episodic shear of granular materials regulated by dilatant strengthening. *Geology 30*, 843–846.

Morgan, B. J. T. & Ray, A. P. G. 1995: Non-uniqueness and inversions in cluster analysis. *Applied Statistics 44*, 117–134.

Neudorf, C. M. 2008: *Relationships between the macroscale sedimentology and micromorphology of glacigenic diamictons in south-central British Columbia*. M.Sc. thesis, Simon Fraser University, 239 pp.

Parkin, G. W. & Hicock, S. R. 1989: Sedimentology of a Pleistocene glacigenic diamicton sequence near Campbell River, Vancouver Island, British Columbia. *In* Goldthwait, R. P. & Matsch, C. L. (eds): *Genetic Classification of Glacigenic Deposits*, 97–116. Balkema, Rotterdam.

Passchier, C. W. & Trouw, R. A. J. 2006: *Microtectonics*. 366 pp. Springer, Berlin.

Phillips, E., Everest, J. & Reeves, H. 2012: Micromorphological evidence for subglacial multiphase sedimentation and deformation during overpressurized fluid flow associated with hydrofracturing. *Boreas*, DOI: 10.1111/j.1502-3885.2012.00261.x.

Phillips, E., van der Meer, J. J. M. & Ferguson, A. 2011: A new 'microstructural mapping' methodology for the identification, analysis and interpretation of polyphase deformation within subglacial sediments. *Quaternary Science Reviews 30*, 2570–2596.

Phillips, E., Merritt, J., Auton, C. & Golledge, N. 2007: Microstructures in subglacial and proglacial sediments: understanding faults, folds and fabrics, and the influence of water on the style of deformation. *Quaternary Science Reviews 26*, 1499–1528.

Piotrowski, J. A., Larsen, N. K. & Junge, F. W. 2004: Reflections on soft subglacial beds as a mosaic of deforming and stable spots. *Quaternary Science Reviews 23*, 993–1000.

Piotrowski, J. A., Larsen, N. K., Menzies, J. & Wysota, W. 2006: Formation of subglacial till under transient bed conditions: deposition, deformation, and basal decoupling under a Weichselian ice sheet lobe, central Poland. *Sedimentology 53*, 83–106.

Piotrowski, J. A., Mickelson, D. M., Tulaczyk, S., Krzyszkowski, D. & Junge, F. W. 2001: Were deforming subglacial beds beneath past ice sheets really widespread? *Quaternary International 86*, 139–150.

Plouffe, A., Bednarski, J. M., Huscroft, C. A., Anderson, R. G. & McCuaig, S. J. 2011: Late Wisconsinan glacial history in the Bonaparte Lake map area, south-central British Columbia; implications for glacial transport and mineral exploration. *Canadian Journal of Earth Sciences 48*, 1091–1111.

Plouffe, A., Bednarski, J. M., Huscroft, C. A. & McCuaig, S. J. 2009: Gold grain content of till in the Bonaparte Lake map area, south central British Columbia (NTS 92P). *Geological Survey of Canada, Open File 6047*, 32 pp.

Reinardy, B. T. I., Hiemstra, J. F., Murray, T., Hillenbrand, C.-D. & Larter, R. D. 2011: Till genesis at the bed of an Antarctic Peninsula palaeo-ice stream as indicated by micromorphological analysis. *Boreas 40*, 498–517.

Roddick, J. A., Muller, J. E. & Okulitch, A. V. 1979: *Fraser River, British Columbia–Washington. Sheet 92. Map 1386A ed.* Geological Survey of Canada, Vancouver, British Columbia, Canada.

Romesburg, H. C. 1984: *Cluster Analysis for Researchers*. 334 pp. Lifetime Learning Publications, Belmont, CA.

Seret, G. 1993: Microstructures in thin sections of several kinds of till. *Quaternary International 18*, 97–101.

Shaw, J. 1979: Genesis of the Sveg tills and Rogen moraines of central Sweden: a model of basal melt-out. *Boreas 8*, 409–426.

Starkey, J. 1977: The contouring of orientation data represented in spherical projection. *Canadian Journal of Earth Sciences 14*, 268–277.

Stokes, C. R., Clark, C. . D., Lian, O. B. & Tulaczyk, S. 2007: Ice stream sticky spots: a review of their identification and influence beneath contemporary and palaeo-ice streams. *Earth-Science Reviews 81*, 217–249.

Thomason, J. F. & Iverson, N. R. 2006: Microfabric and microshear evolution in deformed till. *Quaternary Science Reviews 25*, 1027–1038.

Tipper, H. W. 1971: Multiple glaciation in central British Columbia. *Canadian Journal of Earth Sciences 8*, 743–753.

Truffer, M. & Harrison, W. D. 2006: In situ measurements of till deformation and water pressure. *Journal of Glaciology 52*, 175–182.

Truffer, M., Harrison, W. D. & Echelmeyer, K. A. 2000: Glacier motion dominated by processes deep in underlying till. *Journal of Glaciology 46*, 213–221.

Tulaczyk, S. 1999: Ice sliding over weak, fine-grained tills: Dependence of ice-till interactions on till granulometry. *In* Mickelson, D. M. & Attig, J. W. (eds): *Glacial Processes Past and Present*, 159–177. Geological Society of America, Special Paper 337.

van Vliet-Lanoë, B., Coutard, J. & Pissart, A. 1984: Structures caused by repeated freezing and thawing in various loamy sediments: a comparison of active, fossil and experimental data. *Earth Surface Processes and Landforms 9*, 553–565.

Wentworth, C. K. 1922: A scale of grade and class terms for clastic sediments. *Journal of Geology 30*, 377–392.

Woodcock, N. H. & Naylor, M. A. 1983: Randomness testing in three-dimensional orientation data. *Journal of Structural Geology 5*, 539–548.

Zaniewski, K. & van der Meer, J. J. M. 2005: Quantification of plasmic fabric through image analysis. *Catena 63*, 109–127.

Appendix A: Statistical protocol for cluster analysis of microstructure data

Cluster analysis was performed using the following 6 steps.

(1) All zeros were removed from the dataset using the 'Multiplicative Replacement Strategy' proposed by Martín-Fernández *et al.* (1998a, 2003). This was done to avoid undefined values that would result from the data transformation in Step 2. Thus, if each composition with Z zeros (where $Z>0$) is expressed as a vector x, x is replaced by the composition r using the following expression:

$$r_j = \begin{cases} \partial_j, & \text{if } x_j = 0 \\ \left(1 - \dfrac{\sum k \mid x_k = 0^{\delta_k}}{c}\right)x_j, & \text{if } x_j > 0, \end{cases} \quad (1)$$

where ∂_j is an imputed value equal to 65% of the rounding threshold, and c is the sum constraint equal to 100 (Martín-Fernández *et al.* 2003). Because all values in the dataset are rounded to the nearest percent, the rounding threshold value used here is 0.5%.

(2) Aitchison's (1986) centred log-ratio transformation is applied to the dataset. This transformation removes the constant-sum constraint from the data so that multivariate statistics can be applied. The centred log-ratio transformation is calculated as follows:

$$clr(x) = \left[\ln\left(\frac{x_1}{g(x)}\right), \ldots, \ln\left(\frac{x_D}{g(x)}\right)\right], \quad (2)$$

where D is the number of variables (microstructure types) in composition x, and $g(x)$ is the geometric mean of composition x as calculated below:

$$g(x) = \left(\prod D_{j=1} x_j\right)^{1/D}. \quad (3)$$

(3) All variables in the dataset were standardised to a mean of 0 and a variance of 1 using the formula

$$b_{ij} = (x_{ij} - X_j)/s_j, \quad (4)$$

where X_j and s_j are the arithmetic mean and standard deviation of the jth variable, respectively. This standardisation allows all variables to contribute equally to the clustering process (Romesburg 1984).

(4) A dissimilarity matrix ($ED_{i,h}$) was constructed from the data using Euclidean distances (Martín-Fernández *et al.* 1998b). This matrix is a square, symmetrical matrix where every (i,h)th element represents the Euclidean distance between the ith and hth composition, and is calculated as follows:

$$ED_{i,h} = \sqrt{\sum_{j=1} D(b_{i,j} - b_{h,j})^2}. \quad (5)$$

(5) Agglomerative hierarchical cluster analyses (Everitt 1993) were conducted using multiple linkage methods (Ward's, single, complete, average, McQuitty's, median and centroid) using the 'compositions' package in the statistical software package R (van den Boogaart *et al.* 2008). Dendrograms, or tree diagrams that illustrate the

arrangement of clusters produced by hierarchical clustering, were plotted for each linkage method employed. Because the dendrograms derived from the median and centroid linkage methods contained inversions (Morgan & Ray 1995), they were left out of subsequent analyses.

(6) The cophenetic correlation coefficient ($r_{x,y}$) was calculated for the rest of the linkage methods in order to choose the method that best represents the inter-composition similarity structure inherent in the dissimilarity matrix (Romesburg 1984). The linkage method that yielded the highest cophenetic correlation coefficient (0.86) was the average linkage method. This linkage method was used to cluster the data in Table 3.

Supporting Information

Additional Supporting Information may be found in the online version of this article at the publisher's web-site:

Fig. S1. Microphotograph (A) and microstructure map (B) of thin section S23F30 from Site 23. The yellow unidirectional arrows in (A) point to planar voids that are interpreted to be fissility planes. The black bidirectional arrows in (A) show the orientation of the long-axis of large skeletal grains. The black box in (A) delineates the total thin section area. Microfabric domains are highlighted in (C). In (D), grain orientations are colour-coded according to their orientation, and the four orientation classes are shown in the rose diagram. Grain long-axes that are coloured dark red or dark blue are oriented within 45° of the vertical plane, and those coloured light blue or orange are oriented within 45° of the horizontal plane. A large proportion of grains (light blue) have a gentle apparent plunge down to 347° azimuth. A significant number of sand grains (orange) are aligned subparallel to the apparent long-axis of the largest skeletal grains.

Fig. S2. Microphotograph (A) and microstructure map (B) of thin section S23F31 from Site 23. The yellow unidirectional arrows in (A) point to planar voids that are interpreted to be fissility planes. The yellow bidirectional arrows in (A) show the orientation of the long-axis of large skeletal grains. The black box in (A) delineates the total thin section area. Microfabric domains are highlighted in (C). In (D), grain orientations are colour-coded according to their orientation, and the four orientation classes are shown in the rose diagram. Grain long-axes that are coloured dark red or dark blue are oriented within 45° of the vertical plane, and those coloured light blue or orange are oriented within 45° of the horizontal plane. A large proportion of grains have a gentle apparent plunge down to 184° azimuth.

Fig. S3. Microphotograph (A) and microstructure map (B) of thin section S6F26 from Site 6. The yellow unidirectional arrows in (A) point to planar voids that are interpreted to be fissility planes. The black box in (A) delineates the total thin section area. Microfabric domains are highlighted in (C). In (D), grain orientations are colour-coded according to their orientation, and the four orientation classes are shown in the rose diagram. Grain long-axes that are coloured dark red or dark blue are oriented within 45° of the vertical plane, and those coloured light blue or orange are oriented within 45° of the horizontal plane. The majority of grains have a gentle apparent plunge down to 208° azimuth.

Fig. S4. Microphotograph (A) and microstructure map (B) of thin section S6F27 from Site 6. The black box in (A) delineates the total thin section area. Microfabric domains are highlighted in (C). In (D), grain orientations are colour-coded according to their orientation, and the four orientation classes are shown in the rose diagram. Grain long-axes that are coloured dark red or dark blue are oriented within 45° of the vertical plane, and those coloured light blue or orange are oriented within 45° of the horizontal plane. The majority of grains are oriented within ~45° of the vertical plane.

Fig. S5. Microphotograph (A) and microstructure map (B) of thin section S6F33 from Site 6. The yellow unidirectional arrows in (A) point to planar voids that are interpreted to be fissility planes. The black box in (A) delineates the total thin section area. Microfabric domains are highlighted in (C). Domains oriented perpendicular to the main microfabric orientation are light blue. In (D), grain orientations are colour-coded according to their orientation, and the four orientation classes are shown in the rose diagram. Grain long-axes that are coloured dark red or dark blue are oriented within 45° of the vertical plane, and those coloured light blue or orange are oriented within 45° of the horizontal plane. A large proportion of grains have a gentle apparent plunge down to 22° azimuth.

Fig. S6. Microphotograph (A) and microstructure map (B) of thin section S60F11 from Site 60. The black box in (A) delineates the total thin section area. Microfabric domains are highlighted in (C). In (D), grain orientations are colour-coded according to their orientation, and the four orientation classes are shown in the rose diagram. Grain long-axes that are coloured dark red or dark blue are oriented within 45° of the vertical plane, and those coloured light blue or orange are oriented within 45° of the horizontal plane. The majority of grains are oriented within 45° of the vertical plane.

Fig. S7. Microphotograph (A) and microstructure map (B) of thin section S60F13 from Site 60. The black box in (A) delineates the total thin section area.

Microfabric domains are highlighted in (C). In (D), grain orientations are colour-coded according to their orientation, and the four orientation classes are shown in the rose diagram. Grain long-axes that are coloured dark red or dark blue are oriented within 45° of the vertical plane, and those coloured light blue or orange are oriented within 45° of the horizontal plane.

Fig. S8. Microphotograph (A) and microstructure map (B) of thin section S60F14 from Site 60. The black box in (A) delineates the total thin section area. Microfabric domains are highlighted in (C). Domains with apparent plunges down to the NNW are grey, and those with apparent plunges down to the SSE are blue. In (D), grain orientations are colour-coded according to their orientation, and the four orientation classes are shown in the rose diagram. Grain long-axes that are coloured dark red or dark blue are oriented within 45° of the vertical plane, and those coloured light blue or orange are oriented within 45° of the horizontal plane. A large proportion of grains have a gentle apparent plunge down to 352° azimuth.

Fig. S9. Microphotograph (A) and microstructure map (B) of thin section S60F15 from Site 60. The black box in (A) delineates the total thin section area. Microfabric domains are highlighted in (C). In (D), grain orientations are colour-coded according to their orientation, and the four orientation classes are shown in the rose diagram. Grain long-axes that are coloured dark red or dark blue are oriented within 45° of the vertical plane, and those coloured light blue or orange are oriented within 45° of the horizontal plane.

Fig. S10. Microphotograph (A) and microstructure map (B) of thin section S48F9 from Site 48. The yellow unidirectional arrows in (A) point to planar voids that are interpreted to be fissility planes. The black box in (A) delineates the total thin section area. Microfabric domains are highlighted in (C). In (D), grain orientations are colour-coded according to their orientation, and the four orientation classes are shown in the rose diagram. Grain long-axes that are coloured dark red or dark blue are oriented within 45° of the vertical plane, and those coloured light blue or orange are oriented within 45° of the horizontal plane. The majority of grains have plunges that are within ~45° of the vertical plane.

Fig. S11. Microphotograph (A) and microstructure map (B) of thin section S48F10 from Site 48. The yellow unidirectional arrows in (A) point to planar voids that are interpreted to be fissility planes. The black box in (A) delineates the total thin section area. Microfabric domains are highlighted in (C). In (D), grain orientations are colour-coded according to their orientation, and the four orientation classes are shown in the rose diagram. Grain long-axes that are

coloured dark red or dark blue are oriented within 45° of the vertical plane, and those coloured light blue or orange are oriented within 45° of the horizontal plane.

Fig. S12. Microphotograph (A) and microstructure map (B) of thin section S48F17 from Site 48. The yellow unidirectional arrows in (A) point to systematically oriented planar voids. The black box in (A) delineates the total thin section area. Microfabric domains are highlighted in (C). In (D), grain orientations are colour-coded according to their orientation, and the four orientation classes are shown in the rose diagram. Grain long-axes that are coloured dark red or dark blue are oriented within 45° of the vertical plane, and those coloured light blue or orange are oriented within 45° of the horizontal plane. A large proportion of grains have a gentle apparent plunge down to 17° azimuth.

Fig. S13. Microphotograph (A) and microstructure map (B) of thin section S48F32 from Site 48. The yellow unidirectional arrows in (A) point to systematically oriented planar voids. The black box in (A) delineates the total thin section area. Microfabric domains are highlighted in (C). In (D), grain orientations are colour-coded according to their orientation, and the four orientation classes are shown in the rose diagram. Grain long-axes that are coloured dark red or dark blue are oriented within 45° of the vertical plane, and those coloured light blue or orange are oriented within 45° of the horizontal plane. A large proportion of grains have a gentle apparent plunge down to 357° azimuth.

Fig. S14. Microphotograph (A) and microstructure map (B) of thin section S27F1 from Site 27. The black box in (A) delineates the total thin section area. Microfabric domains are highlighted in (C). Microfabric domains coloured blue are cross-cut by domains coloured grey. In (D), grain orientations are colour-coded according to their orientation, and the four orientation classes are shown in the rose diagram. Grain long-axes that are coloured dark red or dark blue are oriented within 45° of the vertical plane, and those coloured light blue or orange are oriented within 45° of the horizontal plane.

Fig. S15. Microphotograph (A) and microstructure map (B) of thin section S26F28 from Site 26. The yellow unidirectional arrows in (A) point to systematically oriented planar voids. The yellow bidirectional arrows in (A) show the orientations of the long-axis of large skeletal grains. The black box in (A) delineates the total thin section area. Microfabric domains are highlighted in (C). In (D), grain orientations are colour-coded according to their orientation, and the four orientation classes are shown in the rose diagram. Grain long-axes that are coloured dark red or dark blue are oriented within 45° of the vertical plane, and those coloured light blue or

orange are oriented within 45° of the horizontal plane.

Fig. S16. Microphotograph (A) and microstructure map (B) of thin section S26F29 from Site 26. The yellow bidirectional arrows in (A) show the orientations of the long-axis of large skeletal grains. The black box in (A) delineates the total thin section area. Microfabric domains are highlighted in (C). In (D), grain orientations are colour-coded according to their orientation, and the four orientation classes are shown in the rose diagram. Grain long-axes that are coloured dark red or dark blue are oriented within 45° of the vertical plane, and those coloured light blue or orange are oriented within 45° of the horizontal plane.

Fig. S17. Microphotograph (A) and microstructure map (B) of thin section S57F19 from Site 57. The black box in (A) delineates the total thin section area. Microfabric domains are highlighted in (C). In (D), grain orientations are colour-coded according to their orientation, and the four orientation classes are shown in the rose diagram. Grain long-axes that are coloured dark red or dark blue are oriented within 45° of the vertical plane, and those coloured light blue or orange are oriented within 45° of the horizontal plane.